Naval Research Laboratory

Washington, DC 20375-5000

AD-A229 992

NRL Memorandum Report 6754

Key Physics Issues Affecting the Performance of Free Electron Lasers

C. M. TANG, B. HAFIZI,* E. ESAREY, A. TING,
W. MARABLE† AND P. SPRANGLE

Beam Physics Branch
Plasma Physics Division

**Icarus Research*
Bethesda, MD

†*Hampton University*
Hampton, VA 23668

December 20, 1990

REPORT DOCUMENTATION PAGE

Form Approved
OMB No. 0704-0188

1. AGENCY USE ONLY (Leave blank)	2. REPORT DATE	3. REPORT TYPE AND DATES COVERED
	1990 December 20	Interim

4. TITLE AND SUBTITLE

Key Physics Issues Affecting the Performance of Free Electron Lasers

5. FUNDING NUMBERS

47-3137-00
ONR Contract
N00014-87-f-0066

6. AUTHOR(S)

C. M. Tang, B. Hafizi,* E. Esarey,
A. Ting, W. Marable† and P. Sprangle

7. PERFORMING ORGANIZATION NAME(S) AND ADDRESS(ES)

Naval Research Laboratory
Washington, DC 20375-5000

8. PERFORMING ORGANIZATION REPORT NUMBER

NRL Memorandum
Report 6754

9. SPONSORING/MONITORING AGENCY NAME(S) AND ADDRESS(ES)

Office of Naval Research
Arlington, VA 22217

National Institute of Standards and Technology
Gaithersburg, MD 20899

10. SPONSORING/MONITORING AGENCY REPORT NUMBER

11. SUPPLEMENTARY NOTES

*Icarus Research, Bethesda, MD, †Hampton University, Hampton, VA 23668

12a. DISTRIBUTION/AVAILABILITY STATEMENT

Approved for public release; distribution unlimited.

12b. DISTRIBUTION CODE

13. ABSTRACT *(Maximum 200 words)*

Free-electron lasers (FELs) are currently under intense research and development throughout the world for a variety of applications. A number of physics issues place limits on the performance of FELs. These include, among others, i) the generation of high quality, high current electron beams, ii) optical guiding of the generated radiation beam, iii) undulator field errors, and iv) the excitation of sideband radiation. The goal of this paper is to review and discuss these FEL physics issues. The most important component of an FEL is a high quality electron beam. For efficient operation the effective electron beam energy spread must be sufficiently small. The effective energy spread is determined by i) transverse beam emittance, ii) undulator transverse spatial gradients, iii) undulator field error effects, iv) beam space charge effects, v) intrinsic energy spread, and vi) energy stability. Another important aspect of FEL operation is optical guiding of the generated radiation beam. In many proposed FEL experiments, the short wavelength radiation beam will not be confined by a waveguide structure, and the interaction length is required to be long compared to the free-space Rayleigh (diffraction) length. Optical guiding of the generated radiation can, therefore, play a central role in the practical utilization of FELs. However, optical guiding imposes limits on several FEL parameters. These, as well as other constraints, will be discussed in detail, and theoretical criteria and numerical simulations will be presented.

14. SUBJECT TERMS

Free electron laser
Beam quality

15. NUMBER OF PAGES

49

16. PRICE CODE

17. SECURITY CLASSIFICATION OF REPORT	18. SECURITY CLASSIFICATION OF THIS PAGE	19. SECURITY CLASSIFICATION OF ABSTRACT	20. LIMITATION OF ABSTRACT
UNCLASSIFIED	UNCLASSIFIED	UNCLASSIFIED	SAR

CONTENTS

KEY PHYSICS ISSUES AFFECTING THE PERFORMANCE OF FREE ELECTRON LASERS

1 INTRODUCTION

Free-electron lasers (FELs) comprise a class of potentially efficient devices capable of generating high quality coherent radiation, continuously tunable from the microwave region through to the ultraviolet region, at high average and/or high peak power.[1-20] Although the first ideas for the FEL have been known since the original article by Motz[21] in 1951 and the successful experiments by Phillips[22] in 1960, it is the work by Madey[23-25] in the infrared wavelength regime in the 1970s that has made the FEL a serious candidate for a new powerful radiation source.

The FEL is characterized by a relativistic electron beam co-propagating through an undulator field with an input radiation field. If the electron beam is of good quality and has a sufficiently high current density, input radiation at the appropriate frequency will grow, as in the case in an FEL amplifier. The undulator field can be a static periodic magnetic field, a static periodic electric field, or an electromagnetic radiation field. When the gain per pass is low through the undulator, many passes are required for the radiation to reach saturation, as in an FEL oscillator. A schematic of the FEL oscillator is shown in Fig. 1. Here the end mirrors reflect the radiation between the exit and the entrance of the undulator.

The FEL has major differences relative to conventional lasers. The active medium in the FEL is not atoms or molecules but free electrons. The radiation frequency of the FEL is continuously tunable and is not limited to the discrete allowed quantum transitions. The free-electron lasing medium also has the advantage that it can support large amplitude electromagnetic fields that could damage conventional material lasers. In the FEL, the electron kinetic energy is converted into radiation. Some electrons lose kinetic energy, while others gain kinetic energy. Under the appropriate conditions, coherent radiation is generated as electrons on the average lose kinetic energy. Since each electron can gain or lose many photons, the physics can be understood in terms of classical mechanics.

Electrons can lose kinetic energy, as they travel through the interaction region, in two ways. i) Due to electron acceleration by the undulator field alone, magnetic bremsstrahlung radiation is produced. When the the electrons are initially uniformly distributed axially in the beam (not bunched with a periodic wavelength), this spontaneous radiation is incoherent and low in power. ii) The electrons can lose significant kinetic energy due to the force from the "ponderomotive potential well," which is a traveling beat wave formed by the radiation and the undulator fields. When the axial electron beam velocity is approximately equal to the phase velocity of the ponderomotive potential well, the initially uniformly distributed electrons become trapped in the ponderomotive potential well and bunched at the ponderomotive wavelength. The stimulated radiation from the periodic beam bunches is coherent and is many orders of magnitude higher in power than the spontaneous radiation.

Manuscript approved September 4, 1990

The key physics issues concerning the generation of the stimulated coherent radiation are the focus of this paper. These issues include, among others,

i) generation and propagation of high quality, high current electron beams,
ii) optical guiding of the generated radiation beam,
iii) undulator field errors, and
iv) excitation of sideband radiation.

Electron beam sources vary widely in energy, beam quality, current, pulse length, and repitition rate. Radio frequency (rf) driven accelerators, such as rf linacs, microtrons, and storage rings, have peak currents from a few amperes to hundreds of amperes, electron energies up to hundreds of MeV, and electron micro–pulse lengths much shorter than the rf wavelength. Induction accelerators can have many kilo–amperes of current and, currently, have energies up to tens of MeV and pulse lengths of a few tens of nanoseconds to a few microseconds. Electrostatic accelerators usually have low current and low energy, but good beam quality. Lumped parameter modulators usually can provide relatively inexpensive electron beams in the low energy range with pulse durations up to several microseconds and hundreds of amperes of current. Electron beams from pulsed power sources can have very high currents, but they have low energies and pulse durations of tens of nanoseconds. Each of these electron beam sources have been applied to the generation of FEL radiation. The output radiation characteristics vary widely as a result of this wide variation of electron beam sources.

Free-electron laser experiments are conducted all over the world: USA, France, Italy, Germany, USSR, United Kingdom, the Netherlands, China, Japan, and Israel. A recent compilation of the FEL projects around the world is given in Ref. 20. A brief summary of FEL facilities in the United States is given here. Although the conceptual configuration of the FEL is simple, the implimentation was arduous because existing electron beam sources were not designed with FELs in mind. Madey rekindled the interest in the FEL by his experiments in the infrared wavelength with an rf linac at Stanford University.[24–25] Around the same time, Naval Research Laboratory (NRL) and Columbia University collaborated on FEL experiments in the microwave regime with low energy electron beams.[26–27] In the early 1980s, FEL experiments with high energy low current rf linacs were conducted by Los Alamos National Laboratory (LANL), Spectra Technology/Boeing Aerospace Company and TRW/EGG; FEL experiments with high current low energy induction linacs were conducted at Lawrence Livermore National Laboratory (LLNL). Since that time experimental and theoretical research rapidly increased. Research on high power FELs has been carried out at LLNL and at Boeing/LANL. Past, current, and proposed experiments at LANL, TRW, Spectra Technology/Boeing, Stanford University, National Institute of Standards and Technology(NIST)/Naval Research Laboratory(NRL), Duke University, Vanderbilt University, Rocketdyne/Duke, Brookhaven National Laboratory, Bell Laboratories, University of California at Los Angeles (UCLA) and

Lawrence Berkeley Laboratory utilize higher energy beams to produce radiation from the tenth of micron (in the ultraviolet) to the tens of micron (in the infrared) wavelength range. On the other hand, University of California at Santa Barbara(UCSB), Massachusetts Institute of Technology (MIT), Columbia, University of Maryland, University of Central Florida, Hughes and NRL concentrate on FELs utilizing low energy beams to produce radiation from the millimeter to the hundreds of microns in wavelength. Currently, medical and material science user facilities have been established at UCSB, Stanford University, NIST/NRL, Duke University, and Vanderbilt University. The basic FEL theory has mostly been verified with the exception of optical guiding. All the experiments have demonstrated the importance of high quality electron beams. Research efforts are underway to develop FELs in the direction of user-oriented and practical devices.

2 BASIC CONCEPTS OF THE FEL

The basic principles of the FEL are outlined in this section using 1-D models. We will consider a linearly polarized undulator with a field which may be expressed in terms of the vector potential,

$$\mathbf{A}_u(z) = A_u(z)\cos(\int_0^z k_u(z')dz')\hat{\mathbf{e}}_x, \tag{2.1}$$

where $A_u(z)$ and $k_u(z)$ are the slowly varying amplitude and wavenumber of the undulator. The linearly polarized radiation field is

$$\mathbf{A}_r(z,t) = -A(z)\exp[i(kz-\omega t)]\hat{\mathbf{e}}_x/2 + c.c., \tag{2.2}$$

where $A(z) = |A(z)|e^{i\phi(z)}$ is the complex amplitude of the radiation field expressed in polar variables, ω is the frequency, $k = \omega/c$ is the wavenumber, and c.c. denotes the complex conjugate. The electric field is $\mathbf{E}_r = -c^{-1}\partial\mathbf{A}_r/\partial t$, and the magnetic field is $\mathbf{B} = \mathbf{B}_u + \mathbf{B}_r = \nabla\times(\mathbf{A}_u + \mathbf{A}_r)$.

The evolution of the scattered potentials is governed by the wave equations

$$\left(\frac{\partial^2}{\partial z^2} - \frac{1}{c^2}\frac{\partial^2}{\partial t^2}\right)\mathbf{A}_r = -f\frac{4\pi}{c}J_x\hat{\mathbf{e}}_x, \tag{2.3}$$

where J_x is the driving current density, $f = \sigma_b/\sigma_r$ is the filling factor associated with the radiation field, and σ_b and σ_r are the cross-sectional areas of the electron beam and radiation beam, respectively.

The transverse wiggle and axial velocities are obtained by the relativistic force equation for the particles,

$$\frac{d\mathbf{p}}{dt} = -|e|\left(\mathbf{E}_r + \frac{\mathbf{p}\times\mathbf{B}}{\gamma m_0 c}\right), \tag{2.4}$$

where $\mathbf{p} = \gamma m_0 \mathbf{v}$, $\gamma = (1 + \mathbf{p} \cdot \mathbf{p}/m_0^2 c^2)^{1/2} = (1 - \mathbf{v} \cdot \mathbf{v}/c^2)^{-1/2}$ is the total relativistic mass factor, and m_0 is the electron rest mass.

Since the Hamiltonian for (2.4) is not an explicit function of transverse coordinates, conservation of canonical transverse momentum, i.e., $\gamma m_0 \mathbf{v}_\perp - |e|(\mathbf{A}_r + \mathbf{A}_u)/c = constant$, implies that

$$\mathbf{v}_u/c = \frac{1}{\gamma}\frac{|e|}{m_0 c^2}\mathbf{A}_u \tag{2.5a}$$

and

$$\mathbf{v}_r/c = \frac{1}{\gamma}\frac{|e|}{m_0 c^2}\mathbf{A}_r. \tag{2.5b}$$

Figure 2 is a schematic drawing of an electron trajectory in the presence of the undulator field. In most cases of interest $|A_u| >> |A|$, in which case we can write

$$\gamma = \gamma_z \left[1 + \frac{1}{2}\left(\frac{|e|A_u}{m_0 c^2}\right)^2\right]^{1/2}, \qquad \gamma_z = \left(1 - \frac{v_z^2}{c^2}\right)^{-1/2}, \tag{2.6}$$

where v_z is the rms value of the axial velocity.

The energy of an individual electron in the electron beam changes according to

$$\frac{d\gamma}{dt} = -\frac{|e|}{m_0 c^2}(\mathbf{v} \cdot \mathbf{E}_r) = -\frac{|e|}{m_0 c^2}\frac{\partial}{\partial t}\Phi_{pond}(z,t). \tag{2.7}$$

Since the electron wiggle velocity $\mathbf{v}_u$ and the electric field of the radiation $\mathbf{E}_r$ are in the same direction, the electrons in the beam can either gain or lose energy. The electron dynamics can be simply described by its motion in a potential wave, called the ponderomotive potential Φ_{pond},[28-29] where

$$\Phi_{pond}(z,t) = -\frac{|e|\mathbf{A}_u \cdot \mathbf{A}_r}{\gamma m_0 c^2} \simeq -\frac{|e|A_u A}{\gamma m_0 c^2}\frac{e^{i[(k+k_u)z-\omega t+\phi)}}{2} + c.c. \tag{2.8}$$

is formed by the beating of the radiation field with the undulator field. In writing out the last expression for the ponderomotive potential the non-resonant terms have dropped from the right-hand side of Eq. (2.8).

The oscillating electrons at different positions in the beam interact coherently with the radiation field if their velocity v_{z0} is approximately equal to the phase velocity

$$v_{ph} = \omega/(k + k_u) \tag{2.9}$$

of the ponderomotive wave. The resonant frequency for which $v_{z0} = v_{ph}$ is

$$\omega_0 = \frac{(1 + v_{z0}/c)\gamma_0^2 v_{z0} k_u}{(1 + K^2)}, \tag{2.10}$$

where $K = |e|A_u/\sqrt{2}m_0c^2$ is the normalized rmd undulator vector potential amplitude, v_{z0} is the initial rms axial velocity, $\gamma_0 = \gamma_{z0}(1+K^2)^{1/2}$ is the initial relativistic factor, and $\gamma_{z0} = (1 - v_{z0}^2/c^2)^{-1/2}$. The FEL is tunable by varying the magnetic field of the undulator, the period of the undulator, and/or the energy of the electron beam.

Changing to Lagrangian variables $\tilde{\gamma}$ and $\tilde{v}_z$, the equations of motion, as a function of z for an electron with initial phase ψ_0 in the ponderotive potential well, are described by

$$\frac{d\tilde{\gamma}}{dz} = -\frac{\omega/c}{\tilde{\gamma}} f_B K|a| \sin\psi - e_{DC} \tag{2.11}$$

and

$$\frac{d^2\psi}{dz^2} = K_s^2 \left[\sin\psi_R - \sin\psi\right], \tag{2.12}$$

where

$$\psi = \int_0^z \left[(\omega/c) + k_u - \omega/\tilde{v}_z\right] dz' + \phi + \psi_0 \tag{2.13}$$

is the phase of the electron in the ponderomotive wave,

$$K_s = 2k_u \left(\frac{f_B K|a|}{(1+K^2)}\right)^{1/2} \tag{2.14}$$

is the synchrotron wavenumber,

$$\sin\psi_R = \frac{1}{K_s^2}\left[\frac{dk_u}{dz} - \frac{1}{2\tilde{\gamma}^2}\frac{dK^2}{dz} - k\frac{1+K^2}{\tilde{\gamma}^3}e_{DC}\right], \tag{2.15}$$

ψ_R is the resonant phase, e_{DC} is an applied DC accelerating electric field, $a = |e|A/\sqrt{2}m_0c^2$, $f_B = J_0(b) - J_1(b)$ for linearly polarized undulator, J_n is the nth-order Bessel function, and $b = K^2/2(1+K^2)$. The phase of the electron residing at the resonant phase ψ_R does not oscillate.

The FEL efficiency, the ratio of electron energy converted to radiation over the initial electron energy, may be increased above its intrinsic value through various schemes.[29-32] Efficiency can be increased by increasing as a function of the axial distance z, the wavenumber k_u, decreasing the amplitude of the vector potential K, and/or applying dc accelerating electric field, i.e., tapering such that $1 > \sin\psi_R > 0$. The total energy of the electron is a function of the transverse wiggle motion and the mean axial motion such that $\gamma = (1 + K^2)^{1/2}\gamma_z$. Increasing the wavenumber k_u decreases the phase velocity of the ponderomotive wave, Eq. (2.9). The trapped electrons in the ponderomotive

wave will be decelerated, thus kinetic energy associated with axial motion is converted to radiation. Decreasing the amplitude of the vector potential K converts kinetic energy associated with the wiggling motion to radiation, since $v_{u,rms}/c = K/\gamma$. Application of a dc accelerating electric field e_{DC} converts energy from the dc electric field to radiation.

When the taper is too fast, i.e., $\sin\psi_R > 1$, the electrons become free streaming and no longer trapped in the ponderomotive potential well. The efficiency is further explained, and the phase-space diagram is described, in Section 3.2.

The equation governing the amplitude of the radiation is dependent on the electron motion[33]

$$\frac{da}{dz} = i\frac{\omega_b^2/c^2}{2k} f f_B K(z) \left\langle \frac{e^{-i(\psi-\phi)}}{\tilde{\gamma}} \right\rangle, \tag{2.16}$$

where $\langle ... \rangle$ is the ensemble average over all electrons initially within a ponderomotive potential wave, $\omega_b = (4\pi|e|^2 n_0/m_0)^{1/2}$ is the plasma frequency, and n_0 is the electron density. The derivation of (2.16) from (2.3) assumes the slowly varying approximation of the radiation amplitude.

The FEL interaction in 1-D is self-consistently described by Eqs. (2.11)-(2.16). Three of the following sections will discuss how various nonideal effects, such as effective axial energy spread of the electron beam, radiation sideband generation, and undulator field errors, can affect the performance of the FEL. Section 6 shows how radiation guiding can improve the performance of the FEL.

3 ELECTRON BEAM QUALITY

One of the most important factors affecting the performance of the FEL is the electron beam quality. The critical parameters determining the beam quality for the FEL are the peak current and the effective energy spread. The shorter the radiation wavelength, the more stringent are the conditions on beam quality. The efficiency and the gain (or growth rate) are measures of the performance of the FEL. Table I gives the expressions for gain and intrinsic power efficiency in different operational regimes for a cold beam.[34-35] The gain and efficiency will decrease as the effective energy spread increases.

If all the electrons in the beam have the same initial kinetic energy, and propagate along the axis of the undulator, the electron beam can be trapped in the ponderomotive potential well formed by an appropriate radiation field. The trapped electrons on the average lose kinetic energy, which is converted to radiation. The largest efficiency for a given uniform undulator can be obtained when the beam is cold.

For real beams, the axial velocities of the electrons will have a spread. Poor electron beam quality degrades the trapping of the electrons in the ponderomotive potential well. The FEL mechanism fails when a substantial number of electrons overtake and/or lag behind the ponderomotive wave.

The source of some of the effective energy spread is related to the undulator. An experimentally realizable undulator field, which satisfies $\nabla \times \mathbf{B}_u = 0$ and $\nabla \cdot \mathbf{B}_u = 0$, is given by

$$\mathbf{A}_u(x,y,z) = A_x(x,y,z)\cos(\int_0^z k_u(z')dz')\hat{\mathbf{e}}_x, \tag{3.1}$$

where $A_x(x,y,z)$ takes on different forms depending on the shape of the magnetic pole face. For pole faces with no gradient in the x–direction, $A_x(x,y,z) = A_u(z)\cosh(k_u y)$, where $A_u(z)$ and $k_u(z)$ are slowly varying functions of z. This undulator has only weak focusing in the y–direction. Here, we are not considering undulators with field errors (see Sec. 5) or undulators with weak focusing in the x–direction.

3.1 Sources of Effective Energy Spread

In the FEL, the electron beam can be taken to be cold if the rms *axial* velocity of all the electrons in the undulator field is identical. The major factors that contribute to a spread in v_z are i) intrinsic energy spread of the beam from the accelerator, ii) transverse emittance, iii) transverse gradients of the undulator, and iv) undulator field errors. A spread in v_z is related to a spread in γ_z,

$$\frac{\Delta\gamma_z}{\gamma_{z0}} = \gamma_{z0}^2\frac{\Delta v_z}{c}, \tag{3.2}$$

where $\gamma_0 = (1+K^2)^{1/2}\gamma_{z0}$ and $\gamma_z = \gamma_{z0} + \Delta\gamma_z = \left[1-(v_{z0}+\Delta v_z)^2/c^2\right]^{-1/2}$. The contribution to the total effective energy spread by each of the factors above is discussed below.

3.1.1 Intrinsic energy spread

The intrinsic energy spread of the accelerator can come from the cathode, the accelerating structure, or the self–fields of the electron beam. The type of accelerator affects the source of the intrinsic energy spread.

The electron beam can aquire an axial energy spread starting at the cathode.[3] The causes for the spread include i) temperature of the cathode, ii) roughness of the cathode surface, iii) nonuniformity of emission from the cathode surface, iv) asymmetry, nonuniformity, or nonadiabaticity of the applied electric and magnetic fields, and v) the self–field of the electron beam.

The self–field of the beam introduces a difference in energy across the transverse beam profile. The maximum energy spread of the self–field is the difference between the potential of the beam on axis and that on the edge of the beam,

$$\Delta E_{sp} = |e|[\phi_{sp}(r_b) - \phi_{sp}(0)]. \tag{3.3}$$

The self-potential is governed by the equation

$$\nabla^2 \phi_{sp} = -4\pi |e| n_0, \tag{3.4}$$

where n_0 is the electron density. Substituting the solution of ϕ_{sp} from (3.4) into (3.3), we obtain the contribution of self-fields to the intrinsic energy spread

$$\frac{\Delta E_{sp}}{E} = \frac{\nu}{\gamma_0}, \tag{3.5}$$

where Budker's parameter is given by $\nu = \omega_b^2 r_b^2 / 4c^2 = I_b / 17\beta_0$, I_b is peak current in kA, and $\beta_0 = (1 - \gamma_0^{-2})^{1/2}$. The contribution of self-fields to the total energy spread is usually not significant except for high current, low energy beams.

For a well designed cathode, the main source of variation in the intrinsic energy spread among the different accelerators is the accelerating structure. Electrostatic accelerators, linear induction accelerators, microtrons, and storage rings can all have an energy spread much smaller than 1%. Currently, rf linacs typically have an energy spread of approximately 1% due to several possible contributions including the varying accelerating rf field along the length of the electron bunch.

3.1.2 Emittance

Transverse emittance,[36] ϵ, is an important property of beam quality. We define $\pi\epsilon$ to be the area of the smallest ellipse in $x, x' = dx/dz$ transverse phase space which encloses the particles in the beam. It can be expressed approximately as

$$\epsilon \simeq r_b \langle \theta \rangle, \tag{3.6}$$

where r_b is the beam edge radius and θ is the ratio of the perpendicular to the parallel particle velocity in the beam. In writing (3.6) we have assumed that the beam is symmetric and $\epsilon = \epsilon_x = \epsilon_y$. In some accelerators the emittances in the x and in the y planes are different. We will consider the "envelope," or "edge," emittance of the beam

$$\epsilon_x = 4 \left[\langle x^2 \rangle \langle (x')^2 \rangle - (\langle x x' \rangle)^2 \right]^{1/2} = 4\epsilon_{x,rms}. \tag{3.7}$$

This definition is a factor of four larger than the rms emittance.

As energy increases, ϵ decreases; but the normalized emittance

$$\epsilon_n = \beta\gamma\epsilon \tag{3.8}$$

is invariant through the entire linac and beam transport system for linear focusing systems. The FEL requirement on the smallness of ϵ_n is therefore a

specification of the injector system. With new reseach on laser-initiated photo-emission cathodes, future linacs have the potential of reaching higher currents at low emittance.

A frequently used figure of merit for beam quality in FELs is the normalized beam brightness

$$B_n = \alpha_0 I_b / \pi^2 \epsilon_n^2, \tag{3.9}$$

where I_b is the peak beam current and α_0 is a dimensionless number of order unity. For beams with a uniform ellipsoidal cross section, $\alpha_0 = 2$. Table II lists beam parameters associated with various accelerators used for FELs.

Finite transverse emittance affects FELs in two ways: i) it introduces an additional source of effective energy spread, and ii) it causes divergence of the electron beam which limits the radiation wavelength.

Consider an electron beam propagating in the linearly polarized undulator defined by Eq. (3.1). The undulator has a transverse gradient in the y-direction only. Since there is no focusing mechanism in the x-direction, the beam diverges. If the beam is originally cold, i.e., all the electrons have identical energy, the beam divergence in the x-direction causes an effective spread of the velocity in the z-direction, $v_{z,th}$,

$$\left[1 - \left(\frac{v_{z,th}}{c}\right)^2\right]^{-1/2} = \frac{\gamma_{z0}}{\left[1 + \gamma_{z0}^2(\theta_x^2 + \theta_y^2)\right]^{1/2}} \simeq \gamma_{z0}\left[1 - \gamma_{z0}^2(\theta_x^2 + \theta_y^2)/2\right]. \tag{3.10}$$

Consequently, the effective energy spread due to emittance in the x-direction is

$$\frac{\Delta\gamma_{z,th}}{\gamma_{z0}} \simeq \frac{1}{2(1+K^2)}\left(\frac{\epsilon_n}{r_b}\right)^2. \tag{3.11}$$

The contribution of emittance to the total effective axial energy spread is often the limiting factor in applying an accelerator to the generation of short wavelength radiation with the FEL mechanism.

Furthermore, emittance considerations lead to an upper bound on the radiation wavelength based on geometrical overlap of the electron beam and the radiation beam.[3] In the x-direction, the electron beam profile diverges as

$$r_b(z) = r_b(0)[1 + \epsilon^2 z^2 / r_b^4(0)]^{1/2}, \tag{3.12}$$

where $r_b(0)$ is the electron-beam radius at $z = 0$. For a Gaussian radiation mode, the radial extent of the beam is

$$r_s(z) = r_s(0)[1 + \lambda^2 z^2 / \pi^2 r_s^4(0)]^{1/2}, \tag{3.13}$$

where $r_s(0)$ is the radiation -beam waist and λ is the radiation wavelength. If we require $r_b \lesssim r_s$ to ensure good geometrical overlap of the radiation and electron beams, we find the emittance requirement to be

$$\lambda \gtrsim \pi\epsilon. \tag{3.14}$$

For electron beams with weak focusing in both x– and y–directions, this inequality is not applicable; also this inequality is not a sufficient condition for the beam quality requirement in an FEL because of the contribution of emittance to the effective energy spread.

3.1.3 Weak focusing of the undulator

In the y–direction, the weak focusing of the transverse gradient (3.1) of the undulator field causes the electrons to undergo betatron oscillations. The betatron oscillations introduce an effective energy spread[37–39] even for cold beams with zero emittance. The derivation is given below.

The particle motion in the y–direction is governed by

$$\frac{d\tilde{p}_y}{dt} = \frac{|e|}{c}\tilde{v}_x B_z, \tag{3.15}$$

where $B_z = -A_u k_u \sinh(k_u y)\cos(k_u z)$ is the z–component of the magnetic undulator field associated with the realistic undulator and $\tilde{v}_x = v_{x0} + \sqrt{2}K\cosh(k_u\tilde{y})\cos(k_u z)$. Here, the particle orbits $\tilde{y}$ and $\tilde{v}_x$ are functions of $(z, x_0, y_0, v_{x0}, v_{y0})$, where $d/dt = v_z(d/dz)$, x_0 and y_0 are the initial transverse coordinates, and v_{x0} and v_{y0} are the initial transverse velocities. Assuming the fast oscillatory terms, with wavelength equal to half the undulator wavelength, as unimportant and replacing v_z by c at appropriate places, we find that

$$\frac{d^2\tilde{y}}{dz^2} + \frac{K^2}{2\gamma_0^2}k_u \sinh(2k_u\tilde{y}) = 0. \tag{3.16}$$

The small amplitude solution for motion in the y–direction is

$$\tilde{y} = y_b \cos(K_\beta z - \phi_\beta), \tag{3.17}$$

where $K_\beta = Kk_u/\gamma_0$ is the wavenumber of the betatron oscillations,

$$y_b = \left[\left(\frac{\gamma_0 v_{y0}/c}{Kk_u}\right)^2 + y_0^2\right]^{1/2} \tag{3.18}$$

is the amplitude of the betatron oscillation, and

$$\phi_\beta = \cos^{-1}(y_0/y_b) \tag{3.19}$$

is the initial phase of the betatron oscillation.

Applying conservation of energy in a static magnetic undulator field, we can show that the axial velocity of the particles decreases as the amplitude of the betatron oscillations increases. This results in an equivalent energy spread. The axial velocity is found to be

$$\frac{v_z^2}{c^2} = \frac{\gamma_0^2 - 1}{\gamma_0^2} - \frac{2K^2}{\gamma_0^2}\left[\cosh^2(k_u y)\cos^2(k_u z) + \frac{1}{4}[\cosh(2k_u y_0) - \cosh(2k_u y)]\right] - \frac{v_{y0}^2}{c^2}. \tag{3.20}$$

Dropping terms that oscillate at twice the undulator wavenumber, we obtain $v_z = v_{z0} - \Delta v_{z,\beta}$, where $v_{z0} = \beta_0 c - (K^2/2\gamma_0^2)c$ is the mean axial velocity of the electron travelling on axis, $\beta_0 = (1 - \gamma_0^{-2})^{1/2}$, and

$$\frac{\Delta v_{z,\beta}}{c} = \frac{(K_\beta r_b)^2}{2} \tag{3.21}$$

is the amount that the axial velocity is reduced for particles executing betatron oscillations with oscillation amplitude $r_b = y_b$. When the electron beam is properly matched into the undulation, i.e., the beam envelope does not oscillate, then the beam radius is related to the emittance

$$r_b^2 = \epsilon/\pi K_\beta.$$

3.1.4 Total effective axial energy spread

An estimate of the total effective axial energy spread is

$$\frac{\Delta\gamma_{z,th}}{\gamma_{z0}} \simeq \left[\left(\frac{\Delta E}{E}\right)^2 + \left(\frac{(\epsilon_n/r_b)^2}{2(1+K^2)}\right)^2 + \left(\frac{(Kk_u r_b)^2}{2(1+K^2)}\right)^2 + \left(\frac{\Delta\gamma_{z,u}}{\gamma_{z0}}\right)^2 + \ldots\right]^{1/2}. \tag{3.22}$$

The terms on the right-hand side of Eq. (3.22) represent the contributions of the effective energy spread from the intrinsic energy spread of the accelerator, transverse emittance in the x-direction, transverse emittance associated with weak focusing of the undulator in the y-direction, and the undulator field error. The discussion relating to the undulator field errors will be presented in Section 6. The estimate of the total effective axial energy spread (3.22) is approximate because we have assumed that the various contributions to it are statistically independent.

3.2 Acceptable Energy Spread Limit

Estimates of acceptable limits of energy spread can be obtained using simple trapping arguments.[28-29,34-35] In the linear development of the laser radiation the injected axial beam velocity is slightly greater than the phase velocity, $v_{z0} = v_{ph} + \Delta v_z$, where $v_{ph} = \omega/(k + k_u)$ is the axial phase velocity of the longitudinal wave, $v_{ph} >> \Delta v_z > 0$, and Δv_z depends on the particular FEL regime under consideration. This is illustrated in Fig. 3a, where $f_d(\gamma)$ is the electron distribution function at the entrance to the undulator and $\gamma_{ph} = (1 - v_{ph}^2/c^2)^{-1/2}$. The radiation amplitude increases at the expense of the electron's kinetic energy until the electrons become deeply trapped in the longitudinal wave. At this point the radiation field reaches its maximum amplitude, and the average axial electron velocity is approximately given by

$$v_z|_{sat} = v_{ph} - \Delta v_z. \tag{3.23}$$

The electron distribution function at the exit of the undulator is illustrated in Fig. 3b. At saturation the average axial electron velocity has decreased by approximately $2\Delta v_z$. The decrease in the electron beam energy can be directly equated to the increase in radiation energy. For highly relativistic electron beams the decrease in the average electron kinetic energy is $\Delta E = 2\gamma_0\gamma_{z0}^2 m_0 v_{z0}\Delta v_z$ and hence the radiation efficiency is

$$\eta = \frac{\Delta E}{(\gamma_0 - 1)m_0c^2} \simeq 2\gamma_{z0}^2 \Delta v_z/c. \tag{3.24}$$

The longitudinal wave "sees" the beam as monoenergetic if the beam's axial velocity spread is small compared to Δv_z. Requiring $\Delta v_{z,th} << 2\Delta v_z$, we obtain

$$\frac{\Delta\gamma_{z,th}}{\gamma_{z0}} < \eta. \tag{3.25}$$

One way to visualize the trapping condition is to plot the electron distribution in the phase space $(\psi, d\psi/dz)$, where ψ is the relative phase between the electrons and the ponderomotive wave. It is more convenient to visualize the phase space (ψ, γ) or (ψ, γ_z), since the phase ψ is related to the parallel energy γ_z by

$$d\psi/dz = 2k_u(\gamma_z - \gamma_{z0})/\gamma_{z0}. \tag{3.26}$$

Figure 4 is a schematic of the phase space (ψ, γ_z) for uniform undulators. The separatrix, which separates trapped and flowing orbits in the ponderomotive potential, is outlined. The bucket width changes adiabatically as the radiation amplitude grows. The electrons become trapped inside the separatrix. When the electrons rotate to the lowest point of the separatrix, the FEL attains the largest

intrinsic efficiency. The bucket width is approximately the intrinsic efficiency. This is a graphic illustration of the inequality requirement in Eq. (3.25).

In physical terms, the effective energy spread of the beam does not degrade the performance of the FEL if electrons with different axial velocities do not significantly separate at the end of some relevant interaction length. This separation distance must be less than some fraction (dependent on the FEL regime) of the ponderomotive potential wavelength. The wavelength of the ponderomotive potential is $2\pi/(k + k_u)$, which is approximately the radiation wavelength for large γ_{z0}. The effective energy spread criterion can be written as

$$(k_u + k)\Delta v_{z,th} L_{eff}/v_{z0} << 2\pi F, \tag{3.27}$$

where $\Delta v_{z,th}$ is the axial velocity spread, L_{eff} is the effective interaction length, and F is the fraction of the 2π phase the electrons would have traveled in the ponderomotive potential in the effective distance for a cold beam.

In the low gain regime,

$$L_{eff} = L_u, \tag{3.28}$$

and the the electrons obtain the highest efficiency when they traverse almost the whole 2π phase before bunching at the bottom of the pondermomotive potential well, i.e., $F \simeq 1$. Substituting L_u into Eq. (3.27), we obtain

$$\frac{\Delta\gamma_{z,th}}{\gamma_{z0}} << \frac{1}{2N} = \eta, \tag{3.29}$$

where N is the number of undulator periods and η is the intrinsic efficiency.

In the high gain Compton regime, the electron density is sufficiently low so that collective space-charge effects are neglegible. In this regime,[40]

$$L_{eff} \simeq L_e, \tag{3.30}$$

where $L_e = 1/\Gamma$ is the e-folding length, and Γ is the peak growth rate. For the beam to behave as cold, the electrons should not deviate by more than $\pi/2$ in the 2π phase of the ponderomotive well, i.e., $F \simeq 1/4$. Substituting L_e into Eq. (3.27), we obtain

$$\frac{\Delta\gamma_{z,th}}{\gamma_{z0}} << \eta. \tag{3.31}$$

In the Raman regime, the force on the beam electrons due to the collective space-charge wave becomes comparable to the ponderomotive wave. We can estimate the effective interaction length to be the Doppler-shifted plasma wavelength

$$L_{eff} \simeq v_{z0}\gamma_{z0}\sqrt{\gamma_0}/\omega_b, \tag{3.32}$$

where ω_b is the nonrelativistic plasma frequency. Taking $F \simeq 1/4$, we obtain

$$\frac{\Delta\gamma_{z,th}}{\gamma_{z0}} << \eta. \tag{3.33}$$

If the intrinsic efficiency is small, one can tolerate a larger thermal spread in the beam by imposing a large radiation field to initially trap the electrons and extract their kinetic energy by appropriately tapering the undulator. A large fraction of the electrons in the ponderomotive potential well can be trapped, and their energy can be extracted by adiabatically tapering the undulator. Three methods (also known as efficiency enhancement methods) can be applied: decrease the period of the undulator, decrease the vector potential of the undulator, and/or apply an accelerating electric field.

Figure 5 plots the electron distribution function at the entrance and the exit of the undulator. To trap the electrons initially, we require $\langle\gamma_0\rangle = \gamma_R(0)$, where $\gamma_R(z) = [1 + K(z)^2]^{1/2}\gamma_{ph}(z)$ is the γ associated with the resonant electron (see Fig. 5a). At the end of the undulator, the trapped electrons have lost energy (see Fig. 5b).

Figure 6 is a plot of the electrons in the phase space (ψ, γ) and the separatrix for the resonant phase ψ_R that satisfies $0 < \sin\psi_R < 1$. To trap a substantial fraction of the electrons, we require

$$\gamma_R(0) - \Delta\gamma_{trap}/2 < \gamma < \gamma_R(0) + \Delta\gamma_{trap}/2, \tag{3.34}$$

where $\Delta\gamma_{trap} = \Delta\gamma_{z,trap}[1+K^2(z)]^{1/2}$ is the full-width of the bucket, as derived below. Electrons initially trapped within the separatrix remain trapped provided they are adiabatically decelerated. The half-width of the bucket is given by

$$\left(\frac{d\psi}{dz}\right)_{trap} = \pm 2K_s g(\psi_R), \tag{3.35}$$

where K_s is the synchrotron wavenumber (2.14) and

$$g(\psi_R) = [(\psi_R - \pi/2)\sin\psi_R + \cos\psi_R]^{1/2} \tag{3.36}$$

is the reduction in the width of the bucket as a function of the rate of taper. In order to trap a substantial fraction of the electrons, we require the inital depth of the trapping potential $|e|\phi_{z,trap} = \Delta\gamma_{z,trap}(\gamma_0/\gamma_{z0})m_oc^2$ to be larger than the effective axial energy spread, i.e., $|e|\phi_{z,trap} >> \Delta E_{th,total} = \Delta\gamma_{z,th}(\gamma_0/\gamma_{z0})m_oc^2$. By combining (3.26) and (3.35), the full-width of the trapping bucket is

$$\frac{\Delta\gamma_{z,trap}}{\gamma_{z0}} = \frac{1}{k_u}\left|\frac{d\psi}{dz}\right|_{trap} = 4g(\psi_R)\left(\frac{f_B K|a|}{1+K^2}\right)^{1/2}. \tag{3.37}$$

According to Eq. (3.37), even when condition (3.34) is satisfied, the fraction of trapped electrons decreases as the taper increases because the phase-space area decreases.[31]

The effective axial energy spread of the electron beam is unavoidable because it can be introduced through the self-fields, transverse finite emittance, and transverse gradients of the undulator. The above expressions specify the criteria that this effective axial energy spread must satisfy for uniform undulators and for tapered undulators.

Electron beams can possess other energy variations that are also undesirable. The beam can have an energy jitter or an energy droop as a function of time arising from the specific accelerator design. If the electron beam is driven by an rf source, the micro–pulses can have phase jitter relative to the rf source. The beam energy may vary from one macro–pulse to another. All these non–ideal effects degrade the performance of the FEL.

4 RADIATION SIDEBANDS

A major problem affecting FEL performance is the growth of sideband radiation. These sidebands are shifted in frequency from the fundamental radiation and, as they grow, they deplete the electron beam of energy, thus reducing the growth of the fundamental. Sidebands in FELs arise as follows. Electrons trapped in the ponderomotive well perform synchrotron oscillations. Particles trapped near the bottom of the well have a simple harmonic motion with period given by $2\pi/K_s$, where K_s is the synchrotron wavenumber, Eq. (2.14). The oscillations of the trapped electrons generate current components at frequencies shifted from the electron wiggling frequency ck_u by some multiple of the synchrotron frequency cK_s. The synchrotron radiation will appear at frequencies separated from the desired carrier frequency by a multiple of twice the Doppler upshifted synchrotron frequency, i.e.,

$$\Delta\omega_s = c\Delta k_s, \tag{4.1}$$

where $\Delta k_s = 2\gamma_0^2 K_s/(1+K^2)$ and $K_s = 2k_u \left[f_B K|a|/(1+K^2)\right]^{1/2}$. This growth of radiation sidebands, referred to as the sideband instability, was first pointed out by Kroll et al.[31]

The analysis by Kroll et al. revealed the physical basis for this instability to be similar to that in stimulated Raman scattering. The signal wave ω can scatter into an anti-Stokes (higher frequency) wave ω' by extracting energy from the synchrotron motion of the electrons ($\omega + c\Delta k_s \rightarrow \omega'$). Alternatively the signal wave can scatter into a Stokes (lower frequency) component ω' andt at the same time cause the electrons to go into higher energy states of the synchrotron motion ($\omega \rightarrow \omega' + c\Delta k_s$). The growth rate and the relative amplitude of these two processes is determined by the distribution function of the electrons in the

vicinity of v_{ph}. The Stokes process is obviously the more worrisome of the two since it can lead to detrapping of the electrons out the ponderomotive buckets.

Since the work of Kroll et al. more detailed theoretical analyses,[41-45] numerical simulations,[46-57] and experimental observations[45,53,58] of the sideband instabilities have been reported in the literature.

The sideband instability may be important when the electrons can make approximately one or more synchrotron oscillations in the undulator. This is the case for an FEL amplifier after saturation, an FEL operating in the trapped particle mode, or an FEL oscillator with high intra-cavity power.

The synchrotron frequency is a function of the signal wave amplitude $|a|$. Hence, in a high gain FEL where $|a|$ changes rapidly in a synchrotron wavelength, the resonance condition is met only for a short time and the instability is unlikely to be important. For an oscillator, the radiation intensity inside the resonator is substantially higher than that of the extracted radiation, and the amplitude slowly evolves between the cavity mirrors. This situation tends to produce significant levels of sidebands and may possibly lead to diffusion, or Brownian motion, of the electrons out of the ponderomotive well.[31]

Detrapping is obviously a serious effect since it leads to a reduction in gain. Additionally, the sideband instability modulates the ouput signal and consequently increases its spectral width. The performance of the mirrors in an oscillator-type operation can be harmed from the modulation of the wave envelope caused by the sidebands.

A schematic illustration of radiation with a large sideband component is shown in Fig. 7. The amplitude of the electric field is modulated, as shown in Fig. 7a. The wavelength of the modulation is approximately $\lambda_s = 2\pi/\Delta k_s$. The oscillating radiation amplitude leads to an oscillating separatrix, as shown in Fig. 7b. The electrons near the border of the separatrix gradually become lost as the separatrix oscillates. The loss of trapped electrons results in the loss of efficiency.

For an FEL amplifier, sideband modulation can be reduced by a rapid tapering of the undulator field parameters.[45,55,57] In a rapidly tapered FEL amplifier, the ponderomotive bucket changes its position in phase space fast enough to distort the synchrotron orbits of the electrons. A measure of the distortion of electron orbits is given by[31,55,57]

$$R \equiv \left| \frac{cd\gamma_R/dz}{\langle cK_s(\gamma - \gamma_R)\rangle} \right|, \tag{4.2}$$

which is the ratio of the change in energy of the resonant particle $cd\gamma_R/dz$ due to tapering and the change in energy $\langle cK_s(\gamma - \gamma_R)\rangle$ due to synchrotron motion. For a tapering rate corresponding to a resonant phase of $\psi_R = 18°$, the distortion of electron orbits amounts to $R = 25\%$. Together with a decrease in the trapping fraction at fast tapering rates,[52] substantial reduction in sideband modulation was observed in numerical simulations of an FEL amplifier configuration.[55,57]

Several ideas have been put forward in order to reduce the sideband amplitude in FELs; these include

1. Use of mirrors with poor reflectivity at the undesirable sideband wavelengths.[47,51,53-54]
2. Introduction of gratings[56] inside the oscillator cavity so that the sideband radiation is deflected outside the path of the oscillator.
3. Introduction of a gas or liquid with sufficient dispersion to suppress the build-up of the sideband in the cavity.[31]
4. Rapid tapering of the undulator.[45,55,57]
5. Operation in the regime where diffraction is important.[59-60] Theoretical calculations indicate that in this regime the sideband growth rate can be reduced under certain conditions, but not eliminated.

Thus far all analyses of the sideband instability are based on highly simplified models of the FEL wherein many effects are neglected: the evolution of the optical field amplitude, the transverse variation of the optical field, the diffraction of the optical field, etc. Inclusion of these effects and a self-consistent determination of the electron distribution is required before a quantitative comparison between theory and experiment can be attempted.

5 UNDULATOR FIELD ERRORS

Intrinsic magnetic field errors δB are present in any realistic undulator magnet. Such errors are unavoidable and arise from imperfections in the fabrication and assembly of undulator magnets. State-of-the-art undulator construction techniques yield rms field errors on the order[61] $(\delta B/B_u)_{rms} \simeq 0.1 - 0.5\%$. These field errors perturb the electron beam as it propagates through the undulator and lead to i) a random walk of the beam centroid,[62-69] δx, ii) variations in the parallel beam energy,[65-69] $\delta\gamma_z$, and iii) variations in the relative phase of the electrons in the ponderomotive potential,[65-69] $\delta\psi$. If left uncorrected, field errors ultimately decrease free-electron laser (FEL) gain[62-69] (this reduction becomes more significant for long undulators). Reduction in gain may occur from a loss of optical guiding (due to large δx) or from a loss of FEL resonance (due to large $\delta\psi$).

Given the precise functional dependence of the undulator errors $\delta B(z)$ for a given undulator, one may obtain $\delta x(z)$ for that specific undulator. However, one does not always know ahead of time the full functional dependence of $\delta B(z)$. Instead, one may know only certain statistical properties of the field errors, such as the rms value δB_{rms}. Hence, it is useful to consider an ensemble of statistically identical undulators for which the statistical properties of the field errors are known. By performing appropriate averages over this ensemble, one may determine the mean $\langle Q \rangle$ and variance σ for a quantity Q and, hence, determine the most probable range of a single realization of Q. Throughout the following,

$\delta B(z)$ is assumed[66,69] to be a random function with zero mean, and finite variance and with an autocorrelation distance given by $z_{ac} \simeq \lambda_u/2$. Also, in the following, a helical undulator will be assumed, and generalization of the results for a linear undulator is straightforward.[66,69]

5.1 Random Walk of the Beam Centroid

As the electron beam propagates through the undulator, the electrons experience random velocity kicks δv_x via the $v_z \times \delta B_y$ random force. The mean-square centroid motion for the electron beam, including the effects of undulator transverse gradients (weak focusing), is given by[66,69]

$$\langle \delta x^2 \rangle = \frac{D}{k_\beta^2}\left(z - \frac{\sin 2k_\beta z}{2k_\beta}\right), \tag{5.1}$$

where $D = a_u^2 k_u^2 \langle \delta \hat{B}_y^2 \rangle z_{ac}/(2\gamma^2)$, $k_\beta = a_u k_u/\sqrt{2}\gamma_0$ is the betatron wave number of the helical undulator, $\delta \hat{B} = \delta B/B_u$, $a_u = (|e|/m_0c^2)B_u/k_u$ is the normalized vector potential of the helical, undulator and B_u is the ideal undulator peak magnetic field. Physically, the centroid orbits δx and $\delta \beta_x = \delta v_x/c$ represent diffusing betatron orbits characterized by a diffusion coefficient D. Notice that by increasing k_β^2 by additional external focusing, one may, in principle, keep δx_{rms} as small as desired. Furthermore, notice that in the 1-D limit, $(2k_\beta z)^2 << 1$, $\langle \delta \beta_x^2 \rangle = 2Dz$, and $\langle \delta x^2 \rangle = 2Dz^3/3$. Hence, weak focusing (finite k_β) is effective in reducing the asymptotic scaling of the random walk δx_{rms} from $z^{3/2}$ to $z^{1/2}$. To avoid loss of optical guiding it is desirable to keep $\langle \delta x^2 \rangle << r_s^2$, where r_s is the radiation spot size.

5.2 Variations in the Parallel Beam Energy

Not only do the field errors perturb the perpendicular motion of the electrons, they also perturb the parallel motion. This is true since a static magnetic field conserves total electron energy. The parallel motion may easily be calculated[66,69] using the above expressions for the perpendicular motion along with $\beta_z^2 + \beta_\perp^2$ =constant. One may calculate various statistical moments of the parallel motion,[66,69] such as the mean parallel energy variation $\langle \delta \gamma_z \rangle = \langle \gamma_z \rangle - \gamma_{z0}$,

$$\frac{\langle \delta \gamma_z \rangle}{\gamma_{z0}} = -\frac{(1 + a_u^2/4)}{(1 + a_u^2)^2} a_u^2 k_u^2 \langle \delta \hat{B}^2 \rangle z_{ac} z, \tag{5.2}$$

where the limit $(2k_\beta z)^2 >> 1$ has been assumed along with $\langle \delta B_x^2 \rangle = \langle \delta B_y^2 \rangle$.

Statistically, $\langle \delta\gamma_z \rangle$ may be interpreted as an effective energy spread due to field errors.[66,69] This effective energy spread may lead to loss of FEL resonance.

5.3 Deviations in the Relative Phase

To determine how the parallel energy variation affects FEL gain, it is necessary to consider the relative phase ψ of the electrons in the ponderomotive wave, $d\psi/dz \equiv k + k_u - \omega/(c\beta_z)$. In the small signal limit ($a \rightarrow 0$, where a is the normalized radiation field), the deviation in phase $\delta\psi$ due to the field errors is given by

$$\delta\psi \simeq -\frac{\omega}{2c}\int_0^z dz'(2\beta_{\perp 0}\delta\beta_\perp + k_\beta^2 \delta x_\perp^2 + \delta\beta_\perp^2), \tag{5.3}$$

where $\beta_{\perp 0}$ is the ideal wiggle motion in the absence of field errors, i.e., $\beta_{x0} = (a_u/\gamma_0)\cos(k_u z)$, and

$$\delta x = -\frac{a_u k_u}{\gamma k_\beta}\int_0^z dz' \sin k_\beta(z'-z)\delta\hat{B}_y(z') \tag{5.4}$$

and $\beta_x = d\delta x/dz$. Similar expressions hold for δy and $\delta\beta_y$. Statistically averaging over the undulator ensemble gives

$$\langle \delta\psi \rangle \simeq -\frac{a_u^2 k_u^3}{(1+a_u^2)}\langle \delta\hat{B}^2 \rangle z_{ac} z^2, \tag{5.5}$$

where $\langle \delta B_x^2 \rangle = \langle \delta B_y^2 \rangle = \langle \delta B^2 \rangle$ has been assumed. Notice that the mean phase deviation $\langle \delta\psi \rangle$ is independent of the effects of transverse focusing.

Physically, $\delta\psi$ may be interpreted as an oscillation of the ponderomotive well due to field errors. Maintaining FEL resonance requires $\delta\psi$ to be small compared to π, i.e., the width of the well. In the low gain regime, this phase deviation must be kept small over the entire undulator length L_u. Requiring $|\langle \delta\psi(z = L_u) \rangle| < 2\pi$ implies $\delta\hat{B}_{rms} < \alpha/(\pi N)$, where $\alpha^2 = (1+a_u^2)/(2a_u^2)$. A similar condition may be obtained from considerations on the effective energy spread, $\langle \delta\gamma_z \rangle/\gamma_{z0} < \eta = 1/(2N)$. In the high gain regime, the situation is somewhat different, since the length scale over which the FEL resonant interaction occurs is the e-folding length $1/\Gamma$, where Γ is the spatial growth rate of the radiation. Maintaining resonance in the high gain regime corresponds to keeping $\delta\psi$ small over an e-folding length: $|\langle \delta\psi(z = 1/\Gamma) \rangle| < \pi/2$. Since, typically $1/\Gamma << L_u$, one expects the high gain not to be strongly affected by the phase deviation $\delta\psi$ (in contrast to the low gain).

5.4 Degradation of FEL Gain

Quantitatively, the effect of the phase deviation on the FEL gain in the low gain regime may be determined analytically. The normalized mean amplitude gain is related to $\delta\psi$ by the following expression:

$$\langle \hat{G} \rangle = \int_0^z dz' \int_0^{z'} dz''(z' - z'') \langle \sin [\mu k_u (z' - z'') + \Delta\delta\psi] \rangle , \qquad (5.6)$$

where $\Delta\delta\psi \equiv \delta\psi(z') - \delta\psi(z'')$ and $\mu = -N\lambda(\omega - \omega_0)/2\pi c$ is the normalized frequency mismatch parameter. Setting $\Delta\delta\psi = 0$ in the above equation gives the gain in the absence of field errors.

Evaluation of the ensemble average in the above expression is dependent on the statistical distribution of the function $\Delta\delta\psi$. Recall that the phase deviation $\delta\psi$ is proportional to terms that are linear in the field error δB as well as terms that are quadratic in the field error, as indicated by Eq. (5.3). If the field error δB is a Gaussian distributed random variable, then terms quadratic in δB obey a gamma distribution. Hence, if the quadratic terms dominate in the expression for $\delta\psi$, then $\delta\psi$ will tend to be gamma distributed. Assuming $\Delta\delta\psi$ to be approximately gamma distributed allows the ensemble average in Eq. (5.6) to be evaluated using the Rice–Mandel approximation,[62,69,70] yielding

$$\begin{aligned} \langle \hat{G} \rangle = \int_0^z dz' \int_0^{z'} dz''(z' - z'') \left(1 + \langle \Delta\delta\psi \rangle^2 / f^2\right)^{-f/2} \\ \times \sin \left[\mu k_u (z' - z'') + f \tan^{-1} \left(\langle \Delta\delta\psi \rangle / f\right)\right] , \end{aligned} \qquad (5.7)$$

where $f = \langle \Delta\delta\psi \rangle^2 / \left(\langle \Delta\delta\psi^2 \rangle - \langle \Delta\delta\psi \rangle^2\right)$.

It is possible to show that the mean gain is a function of only two parameters, $\langle \hat{G} \rangle = F(\mu, \langle \delta\psi \rangle_{max})$, where $\langle \delta\psi \rangle_{max} = \langle \delta\psi(z = L_u) \rangle$. Furthermore, one can show that the maximum mean gain $\langle \hat{G} \rangle_{max}$ decreases as $\langle \delta\psi \rangle_{max}$ increases.

Equation (5.7) may be evaluated numerically to determine the behavior of the mean gain. Figure 8 illustrates this behavior, in which the mean gain $\langle \hat{G} \rangle$ is plotted as a function of the frequency mismatch μ for several values of rms field error $\delta\hat{B}_{rms}$. The parameters in Fig. 8 correspond to a linearly polarized undulator with $B_u = 5.4$ kG, $\lambda_u = 2.8$ cm, $L_u = 364$ cm, and $\gamma = 350$ in the limit $k_\beta = 0$ (transverse focusing is neglected).

5.5 Beam Steering

One method for reducing the detrimental effect of field errors is through the use of beam steering.[62–69] The effect of steering is to reduce the mean phase deviation by a factor of 1/3, $\langle \delta\psi(L_u)|_{steering} \rangle = (1/3)\langle \delta\psi(L_u)|_{no\ steering} \rangle$, when one steering section is used. It is also possible to calculate $\langle \hat{G} \rangle$ including the effects of steering.

Steering has reduced the variance of the phase deviation by a significant amount. For cases in which $k_\beta \neq 0$, it is possible to show[68,69] that steering reduces the mean phase deviation when the length over which the steering is performed is less than the betatron wavelength, $L_s < \lambda_\beta$. For cases in which $L_s > \lambda_\beta$, beam steering may increase the value of $\langle \delta\psi \rangle$.

This concept may be generalized to the case of multiple beam steering, in which the electron beam is steered back to the axis in several places along the length of the undulator.[63-64,68-69]

Self-consistent, three-dimensional, numerical simulations with undulator field errors and beam steering were performed for a linearly polarized undulator. The amplitude of the undulator field is assumed to be in error with the error of the form of half a period of a sinusoid. The errors of each half sinusoid are uncorrolated with one another, with amplitudes chosen by a random number generator. Figure 9 is a plot of gain versus phase deviation at the end of the undulator calculated for different field errors: $(*)$, no magnetic field errors; $(\circ)$, $(\Delta B/B)_{rms} = 0.4\%$; and $(+)$, $(\Delta B/B)_{rms} = 0.5\%$. The same seed for the random number generator is used for $(\Delta B/B)_{rms} = 0.4\%$ and $(\Delta B/B)_{rms} = 0.5\%$. The parameters of the simulation are for a linearly polarized undulator with $B_u = 5.4$ kG, $\lambda_u = 2.8$ cm, $L_u = 364$ cm, $\gamma_0 = 334.5$, and $\epsilon_n = 9 \times 10^{-4}$ cm rad. The radiation wavelength is $\lambda = 0.25$ μm. The beam is steered on axis at the entrance, the exit, and three equally spaced axial positions in the undulator. The plots show that the gain is inversely related to the phase deviation. The gain degradation is not significant when $\delta\psi < \pi/2$.

5.6 Error Reduction Techniques and Summary

Several methods exist for reducing the detrimental effects of undulator errors. In addition to beam steering, one may consider undulator errors that are correlated.[68] The results discussed above are for undulators with random errors which are assumed to be uncorrelated for separation distances greater than $z_{ac} \simeq \lambda_u/2$. By considering an undulator in which the error for a given magnet pole is correlated to the errors of the surrounding poles, one may construct beneficial correlations that reduce the detrimental effects of the errors.

Alternatively, one may reduce the detrimental effects of the errors by considering an optimal arrangement of the magnet poles.[71-73] That is, the magnet poles are to be arranged in such a way that the detrimental effects of the error of a given pole tend to cancel those of the surrounding poles. More specifically, the magnet poles are arranged in such a way as to minimize an appropriate "cost function." For example, one may choose to arrange the poles such that the magnitude of random walk $|\delta x|$ is minimized, where $\delta x \sim \int dz' \sin k_\beta (z' - z) \delta \hat{B}_y(z')$. (Notice that minimization of $|\int dz \delta B|$ does not correspond to minimization of $|\delta x|$.) However, the results discussed above indicate that a more appropriate cost function is the magnitude of the phase deviation $|\delta\psi|$. Ideally, one would

like to maximize the actual expression for the gain, Eq. (5.6), but the functional dependence of the gain on the field errors appears much too complicated to be of practical use.

The analytical and numerical work discussed above indicates that the phase deviation $\delta\psi$ is the single most important parameter characterizing the effects of undulator errors. Although transverse beam focusing and beam steering are highly effective in controlling the random walk δx (in principle, δx may be kept as small as desired), this is not the case for the phase deviation $\delta\psi$. Transverse beam focusing and beam steering may be used to reduce $|\delta\psi|$ but not eliminate it. The phase deviation leads to a reduction of FEL gain (the low gain regime is affected more strongly than the high gain regime). To avoid significant loss in gain, the above analysis implies that $|\delta\psi| << 2\pi$. Possible error reduction techniques include multiple beam steering, correlation of field errors, and optimal arrangement of magnet poles. An optimal arrangement of poles corresponds to minimization of $|\delta\psi|$, where $\delta\psi$ is given by Eq. (5.3).

6 OPTICAL GUIDING

Unlike the non–ideal effects discussed in Sections 3–5 that degrade the performance of the FEL, optical guiding can improve the gain and the efficiency. The FEL mechanism is most effective when the radiation beam just overlaps the electron beam, such that the filling factor $f = \sigma_b/\sigma_r$ is approximately unity, where σ_b is the area of the electron beam and σ_r is the area of the radiation. For many experiments it is desirable to have the undulator length be much longer than the Rayleigh length. If the radiation can not be confined or guided by a waveguide structure, it is important to overcome free-space diffraction by utilizing an important property of the FEL – radiation guiding.

In the one–dimensional analysis of the FEL, the radiation field, undulator field, and electron beam resonantly couple so as to modify the longitudinal wave number of the radiation field. This resonant interaction, between the coherent radiation and electron beam in the FEL mechanism, can lead to focusing of the radiation beam. This phenomenon was first analyzed for the low gain FEL with transverse effects,[74] where it was shown that the diffractive spreading of the radiation beam could be overcome by a focusing effect arising from the modified index of refraction. Recently optical guiding in FELs operating in the exponential growth regime has been studied in the small signal, exponential growth regime[75–80] to determine the asymptotic behavior of the radiation beam. Figure 10 shows radiation guiding inside and free-space diffraction outside the FEL interaction region for an idealized situation. This radiation focusing phenomenon can play a central role in the practical utilization of high power FELs. Radiation self–focusing provides better coupling between the electron beam and radiation beam over distances longer than a Rayleigh length. This improves FEL gain and efficiency and diminishes losses on the vacuum chamber walls.

To illustrate the concept of radiation self-focusing in the high gain regime, consider a radiation field with a vector potential given by

$$\mathbf{A}_r(r,z,t) = -A(r,z)\exp[i\omega(z/c-t)]\hat{e}_x/2 + c.c., \tag{6.1}$$

where $A(r,z) = |A(r,z)|e^{i\phi(r,z)}$ is the axially symmetric complex amplitude of the radiation field, ω is the frequency, and c.c. denotes the complex conjugate.

The wave equation governing $\mathbf{A}_r$ is

$$\left(\frac{1}{r}\frac{\partial}{\partial r}r\frac{\partial}{\partial r} + \frac{\partial^2}{\partial z^2} - \frac{1}{c^2}\frac{\partial^2}{\partial t^2}\right)\mathbf{A}_r = -\frac{4\pi}{c}J_x\hat{\mathbf{e}}_x, \tag{6.2}$$

where J_x is the driving current density. Using an appropriate expression for J_x, and substituting (6.1) into (6.2), leads to the following reduced wave equation[78]

$$\left(\frac{1}{r}\frac{\partial}{\partial r}r\frac{\partial}{\partial r} + 2i\frac{\omega}{c}\frac{\partial}{\partial z}\right)a(r,z) = \frac{\omega^2}{c^2}[1-n^2(r,z,a)]a(r,z), \tag{6.3}$$

where

$$n(r,z,a) = 1 + \frac{1}{2}\frac{\omega_b^2(r,z)}{\omega^2}\left\langle\frac{e^{-i\psi}}{\gamma_0}\right\rangle\frac{f_B K}{|a(r,z)|} \tag{6.4}$$

is the index of refraction associated with the medium and is, in general, complex and a nonlinear function of $a(r,z)$. Here, $\omega_b(r,z) = [4\pi|e|^2 n_b(r,z)/m_0]^{1/2}$ is the plasma frequency associated with the electron beam density, $a(r,z) = |e|A/\sqrt{2}m_0c^2$ is the normalized radiation vector potential, and $n_b(r,z)$ is the electron beam density. The $\langle\rangle$ denote an ensemble average over all electrons within a ponderomotive wavelength. The imaginary part of n and the real part of n provide the gain and the refraction properties of the radiation, respectively. Gain and refraction are coupled in FELs.

Figure 11 illustrates the refractive property of the FEL in the low gain regime when the input radiation has a flat wavefront at the entrance of the undulator. Inside the electron beam, the FEL interaction produces an index of refraction greater than one, $n > 1$. The wavefront becomes curved and radiation builds up on the axis.

To illustrate the property of radiation self-focusing, the following source-dependent expansion (SDE)[78-81] for radiation field $a(r,z)$ is convenient:

$$a(r,z) = \sum_m a_m(z)L_m\left(\frac{2r^2}{r_s(z)^2}\right)\exp\left[-[1-i\alpha(z)]\frac{r^2}{r_s^2(z)}\right], \tag{6.5}$$

where $m = 0,1,2,\cdots$. In Eq. (6.5), $a_m(z)$ are the complex amplitude coefficients, $r_s(z)$ is the radiation spot size, $\alpha(z)$ is related to the radius of curvature of the

radiation beam wavefront, $R = -(\omega/2c)r_s^2/\alpha$ is the radius of curvature, and L_m is the Laguerre polynomial.

Let us assume that the radiation beam is approximately Gaussian and the a_0 mode is a good approximation to the radiation field. The unknown quantities a_m, r_s, and α can be solved self-consistently.[78-81]

The beam is called perfectly guided when self-similar solutions exist, i.e., the spot size and the curvature remain constant. The complex amplitude of the radiation grows exponentially,

$$a(r,z) = a_0(z=0)\exp[(\Gamma - i\Delta k)z]\exp\left[-r^2\left(\frac{1}{r_s^2} + i\frac{k}{2R}\right)\right], \qquad (6.6)$$

where Γ is the growth rate and Δk is the phase shift. Guided radiation beams can be obtained in the small signal, exponential gain regime for a uniform electron beam radius. In the trapped particle regime, the radiation spot size will increase but at a rate slower than free-space diffraction for the same beam.

Solutions of r_s, α, Γ, and Δk may be obtained for Gaussian and parabolic electron beam transverse density profiles:[79-80]

$$n_b(r) = \begin{cases} n_0 \exp\left(-r^2/r_b^2\right), & \text{Gaussian electron beam;} \\ n_0\left(1 - r^2/r_b^2\right), & \text{parabolic electron beam;} \end{cases} \qquad (6.7)$$

where n_0 is the electron beam density on axis. These solutions are functions of the filling factor, defined as

$$f = \sigma_b/\sigma_r, \qquad (6.8)$$

where

$$\sigma_b = \begin{cases} \pi r_b^2, & \text{Gaussian electron beam;} \\ \pi r_b^2/2, & \text{parabolic electron beam;} \end{cases} \qquad (6.9)$$

and $\sigma_r = \pi r_s^2$. Radiation guiding properties of Gaussian and parabolic electron beams are found to be similar. An explicit expression for the filling factor may be obtained by solving an implicit equation derived in Refs. 79 and 80. Consequently, the expressions for the radius of curvature, R, the growth rate Γ, the phase shift Δk, and the intrinsic efficiency η can be evaluated directly in terms of the input parameters.

For a Gaussian electron beam profile, the equation governing the filling factor can be written as[79]

$$f^3 + f^2 + \left(\frac{1}{4} - \frac{3}{4}d\right)f - \frac{d}{2} = 0, \qquad (6.10)$$

where

$$d = \left(\frac{3\sqrt{2}k\Gamma_0\sigma_b}{5\pi}\right)^{2/3}, \qquad (6.11)$$

$$\Gamma_0 = (5/6 f_B K k_u)(\nu/\gamma)^{1/2}(1+K^2)^{-1/2}, \tag{6.12}$$

$k = \omega/c$, and $\nu = I_b(kA)/17\beta_0$. The filling factor is a function only of one dimensionless parameter d. The solution for the filling factor is

$$f \simeq \left(\frac{3d}{4}\right)^{1/2} - \frac{1}{6} \tag{6.13}$$

for $d >> 1/27$. Equation (6.13) is a very good expression for the filling factor for all practical parameters of interest.

For the parabolic electron beam profile, the equation for the filling factor can be written as[80]

$$2f^4(4f-1)^4(2f-1) - (6f-1)^3 d^3 = 0. \tag{6.14}$$

For $f > 1/2$, the approximate solution to the above equation is

$$f \simeq \frac{3}{4} d^{1/2}. \tag{6.15}$$

With the appropriate explicit expressions for the filling factor, expressions can be determined for the radius of curvature R, the growth rate Γ, the phase shift Δk, and the intrinsic efficiency η, and these are summarized in Table III. For large filling factors ($f > 1$), the scaling relations reduce to those of the 1-D limit. For $f = 1$, the growth rate is Γ_0 for parabolic electron beam profile.

Optical guiding is important when the interaction length is much longer than the Rayleigh length and the Rayleigh length is longer than the e-folding length, i.e.,

$$L_u >> z_R > 1/\Gamma, \tag{6.16}$$

where $z_R = \pi r_s^2/\lambda$ is the Rayleigh length associated with the radiation spot size. Substituting the expressions from Table III, we obtain

$$N_e >> 0.68(k\sigma_b\Gamma_0)^{1/3} > 1, \tag{6.17}$$

where $N_e = L_u/\Gamma$ is the possible number of e-folds in the interaction length. Since it is desirable to make the FEL compact, the FEL undulator length can be reduced by using a shorter undulator wavelength, which leads to the requirement of small electron beam area σ_b. To satisfy the inequality (6.17), the beam current must increase as σ_b decreases, thus the beam brightness must increase.

Using arguments based on electron trapping in the ponderomotive wave, the intrinsic efficiency in the exponential cold Compton regime may be written as[79-80]

$$\eta \simeq \Delta k/k_u. \tag{6.18}$$

The relevant expressions for efficiency are summarized in Table III.

The radiation guiding property of the FEL can overcome the reduction of gain and efficiency caused by free-space diffraction. For FEL configurations to take advantage of optical guiding, the radiation has to grow sufficiently fast that (6.17) is satisfied. At the same time high beam quality is required, such that the effective axial energy spread is much less than the intrinsic efficiency, inequality (3.25), where the efficiency is defined by (6.18).

7 SUMMARY

The above discussion has delineated the key physics issues affecting the performance of the FEL: i) electron beam quality, ii) optical guiding of the radiation beam, iii) radiation side band, and iv) undulator field errors. Perhaps the most critical component of an FEL is a high quality electron beam. Several sources exist for preducing an effective energy spread of the electron beam, in addition to the intrinsic energy spread: transverse beam emittance, undulator transverse spatial gradients, and undulator field errors. The electron beam can be considered to be cold when the effective axial energy spread is much less than the intrinsic efficiency. Large energy spreads can significantly reduce the gain and efficiency. Radiation sidebands and undulator field errors can also reduce the gain and efficiency. Several methods may be utilized to overcome these detrimental effects. Radiation diffraction can also reduce the gain and efficiency. The electron beam, the radiation field, and the undulator field resonantly couple in the FEL to modify the longitudinal wave number of the radiation field and the corresponding index of refraction. This allows the radiation beam to become "guided," i.e., the spot size r_s remains constant as the radiation propagates. Radiation guiding provides better coupling between the electron beam and the radiation beam over distances longer than a Rayleigh length, thus improving both gain and efficiency.

The physics issues affecting the performance of the FEL are not limited to the topics discussed above. Examples of other technological and practical areas of the FEL that require attention are electron pulse slipping relative to the radiation pulse, sensitivity of growth rates and pulse shape on mirror detuning, transverse mode structure and mode purity, mirror degradation due to UV radiation, resonator design in a high gain oscillator, electron beam jitter, energy droop, electron beam transport, etc.

The FEL is rapidly becoming an application-oriented coherent radiation source. The principles of FELs, except for radiation guiding, have been demonstrated by the FEL experiments. The dominant limitation in extending the FEL to shorter wavelengths and higher powers is the beam quality of currently existing accelerators. Research efforts on high brightness cathodes, micro-undulators, and improved mirrors will extend the performance of the FEL in the future.

Acknowledgments

The authors would like to thank T. Godlove. The work is supported by the Office of Naval Research (ONR) and by the National Institute of Standards and Technology, which is funded by the Strategic Defense Initiative Office through ONR Contract No. N00014-87-f-0066.

8 REFERENCES

[1] T. C. Marshall, *Free Electron Lasers* (Macmillan, New York, 1985).

[2] P. Sprangle and T. Coffey, Physics Today **37**, 44 (1984).

[3] C. W. Roberson and P. Sprangle, Phys. Fluids **B1**, 3 (1989).

[4] H. P. Freund and R. K. Parker, Sci. Am. April 1989, p. 84.

[5] T. F. Godlove and P. Sprangle, Particle Accelerators **34**, 169 (1990).

[6] *Free-Electron Generators of Coherent Radiation*, Physics of Quantum Electronics, Vol. 7, edited by S. F. Jacobs, H. S. Pilloff, M. Sargent III, M. O. Scully, and R. Spitzer (Addison-Wesley, Reading, MA, 1980).

[7] *Free-Electron Generators of Coherent Radiation*, Physics of Quantum Electronics, Vol. 8 and 9, edited by S. F. Jacobs, G. T. Moore, H. S. Pilloff, M. Sargent III, M. O. Scully, and R. Spitzer (Addison-Wesley, Reading, MA, 1982).

[8] *Bendor Free Electron Laser Conference*, Bendor, Sept.-Oct. 1982, J. Physique, Colloque **C1**, supplement au n^o 2, Tome 44 (les editions de physique, Lew Ulis Cedex, France, 1983).

[9] *Free-Electron Generators of Coherent Radiation*, SPIE Vol. **453**, Proc. of the Free Electron Laser Conference, Orcas Island, WA, June-July 1984, edited by C. A. Brau, S. F. Jacobs, and M. O. Scully (SPIE, Bellingham, WA, 1984).

[10] *Free Electron Lasers*, Proc. of the 1984 Free Electron Laser Conference, Castelgandolfo (Rome), Italy, Sept. 1984, edited by J. M. J. Madey and A. Renieri (North-Holland, Amsterdam, 1985).

[11] *Free Electron Lasers*, Proc. of the Seventh Intl. Conf. on Free Electron Lasers, Tahoe City, CA, Sept. 1985, edited by E. T. Scharlemann and D. Prosnitz (North-Holland, Amsterdam, 1986).

[12] *Free Electron Lasers*, Proc. of the Eighth Intl. Free Electron Laser Conf., Glasgow, United Kingdom, Sept. 1986, edited by M. Poole (North-Holland, Amsterdam, 1986).

[13] *Free Electron Lasers*, Proc. of the Ninth Intl. Free Electron Laser Conf., Williamsburg, VA, Sept. 1987, edited by P. Sprangle, J. Walsh, and C. M. Tang (North-Holland, Amsterdam, 1988).

[14] *Free Electron Generation of Extreme Ultraviolet Coherent Radiation*, AIP Conf. Proc. No. 118, edited by J. M. J. Madey and C. Pellegrini (American Institute of Physics, New York, 1984).

[15] *Free Electron Laser Handbook*, edited by W. Colson, C. Pellegrini, and A. Renieri (North-Holland, Amsterdam, in press).
[16] A. Szoke, editor, *Special Issue on Free-Electron Lasers*, IEEE J. Quantum Electron. **QE-17**, 1326 (1981).
[17] L. R. Elias and W. B. Colson, editors, *Special Issue on Free-Electron Lasers*, IEEE J. Quantum Electron. **QE-19**, 256 (1983).
[18] V. L. Granatstein and C. W. Roberson, editors, *Special Issue on Free-Electron Lasers*, IEEE J. Quantum Electron. **QE-21**, 804 (1985).
[19] C. A. Brau and B. E. Newnam, editors, *Special Issue on Free-Electron Lasers*, IEEE J. Quantum Electron. **QE-23**, 1468 (1987).
[20] J. M. Ortega, Synchrotron Radiation News **3**, 26 (1990).
[21] H. Motz, J. Appl. Phys. **22**, 527 (1951).
[22] R. M. Phillips, IRE Trans. Electron Devices **7**, 231 (1960).
[23] J. M. J. Madey, J. Appl. Phys. **42**, 1906 (1971).
[24] L. R. Elias, W. M. Fairbanks, J. M. J. Madey, H. A. Schwettman, and T. I. Smith, Phys. Rev. Lett. **36**, 717 (1976).
[25] D. A. G. Deacon, L. R. Elias, J. M. J. Madey, G. J. Ramian, H. A. Schwettman, and I. I. Smith, Phys. Rev. Lett. **38**, 892 (1977).
[26] T. C. Marshall, S. Talmadge, and P. Efthimion, Appl. Phys. Lett. **31**, 320 (1977); R. M. Gilgenbach, T. C. Marshall, and S. P. Schlesinger, Phys. Fluids **22**, 971 (1979).
[27] D. B. McDermott, T. C. Marshall, R. K. Parker, and V. L. Granatstein, Phys. Rev. Lett. **41**, 1368 (1978).
[28] P. Sprangle, R. A. Smith, and V. L. Granatstein, *Infrared and Millimeter Waves*, Vol. I, edited by K. J. Button (Academic Press, New York, 1979) p. 279.
[29] P. Sprangle, C. M. Tang, and W. M. Manheimer, Phys. Rev. Lett. **43**, 1932 (1979); P. Sprangle, C. M. Tang and W. M. Manheimer, Phys. Rev. **A21**, 302 (1980); P. Sprangle, C. M. Tang, and W. M. Manheimer, in Ref. 6, Chap. 8, p. 207.
[30] N. M. Kroll, P. L. Morton, and Rosenbluth, in Ref. 6, p.113.
[31] N. M. Kroll, P. L. Morton, and Rosenbluth, IEEE J. Quantum Electron. **QE-17**, 1436 (1981).
[32] A. T. Lin and J. M. Dawson, Phys. Rev. Lett. **42**, 1670 (1979).
[33] C. M. Tang and P. A. Sprangle, IEEE J. Quantum Electron. **QE-21**, 970 (1985).
[34] P. Sprangle, C. M. Tang, and C. W. Roberson, Nucl. Instrum. Methods in Phys. Research **A239**, 1 (1985).
[35] P. Sprangle, C. M. Tang, and C. W. Roberson, in Ref. 15.
[36] J. D. Lawson, *The Physics of Charged Particle Beams* (Oxford U.P., London, 1977).
[37] T. I. Smith and J. M. J. Madey, Appl. Phys. **B27**, 195 (1982).
[38] C. M. Tang, Proc. of the Intl. Conf. on Lasers '82, New Orleans, LA, 1982, edited by R. C. Powell (STS, McLean, VA, 1983), p. 164.

[39] P. Sprangle and C. M. Tang, NRL Memo Report 4663 (1981).
[40] C. Pellegrini and J. Murphy, Optics Comm. **53**, 197 (1985); C. Pellegrini and J. Murphy, in Ref. 15.
[41] N. M. Kroll and M. N. Rosenbluth, in Ref. 6, p.147.
[42] R. C. Davidson and J. S. Wurtele, Phys. Fluids **30**, 557 (1987).
[43] S. Riyopoulos and C. M. Tang, Phys. Fluids **31**, 1708 (1988).
[44] S. Riyopoulos and C. M. Tang, Phys. Fluids **31**, 3387 (1988).
[45] A. Bhattacharjee, S. Y. Cai, S. P. Chang, J. W. Dodd, and T. C. Marshall, Nucl. Instrum. Methods in Phys. Research **A285**, 158 (1989).
[46] A. T. Lin, in Ref. 7, p. 867.
[47] C. Goldstein and W. B. Colson, Proc. of the Intl. Conf. on Lasers '82, New Orleans, LA, 1982, edited by R. C. Powell (STS, McLean, VA, 1983), p. 218.
[48] C. M. Tang and P. Sprangle, in Ref. 9, p.11.
[49] D. C. Quimby, J. M. Slater, and J. P. Wilcoxon, IEEE J. Quantum Electron. **QE–21**, 979 (1985).
[50] R. A. Freeman and W. B. Colson, Optics Comm. **52**, 409 (1985).
[51] J. C. Goldstein, B. E. Newnam, R. W. Warren, and R. L. Sheffield, Nucl. Instrum. Methods in Phys. Research **A250**, 147 (1986).
[52] W. B. Colson, Nucl. Instrum. Methods in Phys. Research **A250**, 168 (1986).
[53] J. C. Goldstein, B. E. Newnam, and R. W. Warren, Nucl. Instrum. Methods in Phys. Research **A272**, 150 (1988).
[54] R. W. Warren and J. C. Goldstein, Nucl. Instrum. Methods in Phys. Research **A272**, 155 (1988).
[55] B. Hafizi, A. Ting, P. Sprangle, and C. M. Tang, Phys. Rev. **A38**, 197 (1988).
[56] R. Toker, J. C. Goldstein, and B. McVay, IEEE J. Quantum Electron. **24**, 856 (1988); R. Toker, B. McVay, L. Todd, and G. Gallatin, IEEE J. Quantum Electron. **25**, 73 (1989).
[57] B. Hafizi, A. Ting, P. Sprangle, and C. M. Tang, Phys. Rev. Lett. **64**, 180 (1990).
[58] T. Masud, T. C. Marshall, S. P. Schlesinger, and F. G. Yee, Phys. Rev. Lett. **56**, 1567 (1986); T. Masud, T. C. Marshall, S. P. Schlesinger, F. G. Yee, W. M. Fawley, E. T. Scharlemann, S. S. Yu, A. M. Sessler, and E. J. Sternback, Phys. Rev. Lett. **58**, 763 (1987).
[59] T. M. Antonsen Jr. and G. Laval, Phys. Fluids **B1**, 1721 (1989).
[60] W. Sharp and S. Yu, Phys. Fluids **B2**, 581 (1990).
[61] K. E. Robinson, D. C. Quimby, and J.M. Slater, IEEE J. Quantum Electron. **QE–23**, 1497 (1987); K.E. Robinson, D.C. Quimby, J.M. Slater, T.L. Churchill, and A.S. Valla, Nucl. Instrum. Meth. **A259**, 62 (1987).
[62] B.M. Kincaid, J. Opt. Soc. Am. **B 2**, 1294 (1985).
[63] C.J. Elliott and B.D. McVey, in *Adriatico Research Conf. Proc. Undulator Magnets for Synchrotron Radiation and Free Electron Lasers*, Trieste,

Italy, June 1987, edited by R. Bonifacio, L. Fonda and C. Pellegrini (World Scientific, London, 1988) p. 142.
[64] H.D. Shay and E.T. Scharlemann, Nucl. Instrum. Meth. **A272**, 601 (1988).
[65] E. Esarey, W. Marable, C.M. Tang, and P. Sprangle, Bull. Am. Phys. Soc. **33**, 1066 (1988).
[66] E. Esarey, W. Marable, and C.M. Tang, J. Appl. Phys. **67**, 2210 (1990).
[67] W. Marable, E. Esarey, and C.M. Tang, submitted to Phys. Rev. A.
[68] W. Marable, E. Esarey, and C.M. Tang, submitted to Phys. Fluids; W. Marable, E. Esarey, and C.M. Tang, to be published in *Proc. of the 11th Intl. Free Electron Laser Conf.*, Naples, FL, August 1989.
[69] E. Esarey, W. Marable, and C.M. Tang, to be published in *Proc. of the 11th Intl. Free Electron Laser Conf.*, Naples, FL, August 1989.
[70] S.O. Rice, Bell Syst. Tech. J. **24**, 46 (1945); L. Mandel, Proc. Phys. Soc. **74**, 233 (1959).
[71] A. Cox and B. Youngman, Proc. SPIE **582**, 91 (1986).
[72] G. Rakowsky, B. Bobbs, and D.C. Slater, Bull. Am. Phys. Soc. **33**, 908 (1988).
[73] M.S. Curtin, A. Bhowmik, W.A. McMullin, S.V. Benson, J.M.J. Madey, B.A. Richman, and L. Vintro, Nucl. Instrum. Meth. **A272**, 91 (1988).
[74] P. Sprangle and C. M. Tang, Appl. Phys. Lett. **39**, 677 (1981); P. Sprangle and C. M. Tang, AIAA J. **19**, 1164 (1981); C. M. Tang and P. Sprangle, in Ref. 7, p. 627.
[75] G. T. Moore, Opt. Comm. **52**, 46(1984); G. T. Moore, Ibid. **54**, 121 (1985); G. T. Moore, Nucl. Instrum. Methods in Phys. Research **239**, 19 (1985).
[76] E. T. Scharlemann, A. M. Sessler, and J. S. Wurtele, Phys. Rev. Lett. **54**, 1925 (1985).
[77] M. Xie and D. A. G. Deacon, Nucl. Instrum. Methods in Phys. Research **A250**, 426 (1986).
[78] P. Sprangle, A. Ting, and C. M. Tang, Phys. Rev. Lett. **59**, 202 (1987); P. Sprangle, A. Ting, and C. M. Tang, Phys. Rev. **A30**, 2773 (1987).
[79] B. Hafizi, P. Sprangle, and A. Ting, Phys. Rev. **A36**, 1739 (1987).
[80] P. Sprangle, A. Ting, B. Hafizi, and C. M. Tang, Nucl. Instrum. Methods in Phys. Research **A272**, 536, 1988.
[81] C. M. Tang, P. Sprangle, A. Ting, and B. Hafizi, J. Appl. Phys. **66**, 1549 (1989)
[82] Private communications: T. J. Orzechowski (LLNL), R. Sheffield (LANL), G. Ramian (UCSB), T. I. Smith (Stanford), B. Danly (MIT), and G. Bekefi (MIT).
[83] L. R. Elias and G. Ramian, Proc. of the Intl. Conf. on Lasers '82, New Orleans, LA, 1982, edited by R. C. Powell (STS, McLean, VA, 1983), p. 152.
[84] R. G. Johnson, et al., to be published in *Proc. of the 11th Intl. Free Electron Laser Conf.*, Naples, FL, August 1989.

[85] T. I. Smith, J. C. Frisch, R. Rohatgi, H. A. Scwettman, and R. L. Swent, to be published in *Proc. of the 11th Intl. Free Electron Laser Conf.*, Naples, FL, August 1989.

[86] S. V. Benson, W. S. Fann, B. A. Hooper, J. M. J. Madey, E. Szarmes, B. Richman, and L. Vintro, to be published in *Proc. of the 11th Intl. Free Electron Laser Conf.*, Naples, FL, August 1989.

[87] D. Goodman, D. Birx, D. Clarke, R. Klinkowstein, R. Shefer, W. Menninger, B. Danly, and R. Tempkin, to be published in *Proc. of the 11th Intl. Free Electron Laser Conf.*, Naples, FL, August 1989.

[88] A. DiRienzo and G. Bekefi, SPIE **1226**, 209 (1990).

Table I: 1–Dimensional Expressions for Gain and Intrinsic Power Efficiency

FEL operating regime	Growth rate (Power gain)	Intrinsic power efficiency
High–gain Compton	$\sqrt{3}\left(\frac{\pi}{2}\frac{f}{\lambda_u}\frac{\nu}{\gamma_0}\right)^{1/3}\left(\frac{f_B K}{\gamma_0 r_b}\right)^{2/3}$	$\left(\frac{f}{16\pi^2}\frac{\nu}{\gamma_0}\right)^{1/3}\left(\frac{\lambda_u f_B K}{r_b \gamma_0}\right)^{2/3}$
Raman	$\left(\frac{\pi\gamma_{z0} f}{r_b \lambda_u}\right)^{1/2}\left(\frac{\nu}{\gamma_0}\right)^{1/4}\frac{f_B K}{\gamma_0}$	$\frac{1}{\pi\gamma_{z0}}\left(\frac{\nu}{\gamma_0}\right)^{1/2}\frac{\lambda_u}{r_b}$
Low–gain Compton	$\pi f \frac{\nu}{\gamma_0}\left(\frac{f_B K \lambda_u}{\gamma_0 r_b}\right)^2 N^3$	$\frac{1}{2N}$

$\nu = (\omega_b r_b/2c)^2 = I_b/17\beta_0$	Budker's parameter
I_b	peak current in kA
N	number of undulater periods
r_b	electron beam radius
$f = \sigma_b/\sigma_r$	filling factor
$\sigma_b = \pi r_b^2$	cross-sectional area of the electron beam
σ_r	cross-sectional area of the radiation beam
$\omega_b = (4\pi\|e\|^2 n_0/m_0)^{1/2}$	the plasma frequency
n_0	the electron density
$f_B = J_0(b) - J_1(b)$	$b = K^2/2(1+K^2)$
$K = (\|e\|/m_0 c^2)(A_u/\sqrt{2})$	$\gamma_{z0} = \gamma_0/(1+K^2)$
$\beta_0 = (1-\gamma_0^{-2})^{1/2}$	

Table II: Accelerators Used in FELs[3,5,82-88]

Location (type)	Voltage [MeV]	Current[a] [A]	ϵ_n^b [cm rad]	$\Delta E(t)/E$ [%]	Brightness[c] [A/cm^2 rad^2]
UCSB (electrostatic)	3–6	2 (20)[d]	1.2×10^{-3}	$< 10^{-3}$	2.8×10^5
Duke (rf linac/Mark III)	27–44	30	$(4 \times 10^{-4})^e$	30 kV ps[f]	$(1.9 \times 10^7)^g$
LANL (rf linac)	20	250	1.6×10^{-2}	1.0	2.0×10^5
Boeing (rf linac)[j]	150	250	5.0×10^{-3}	1.0	2.0×10^6
Osaka (rf linac)	34	600	6.7×10^{-3}	1.0	2.8×10^6
NRL (induction linac)	0.7	150	6.2×10^{-2}	2.0	8.0×10^3
LLNL (ETA induction linac)	3.5	850	0.3	0.035	2.0×10^3
MIT (SNOMAD induction linac)	1.2	1000	5.0×10^{-2}	...	8×10^4
MIT (pulserad Marx system)	1.5	425	$(6.0 \times 10^{-2})^h$	0.019	$(1.1 \times 10^4)^h$
LLNL (ATA induction linac)	45	500–1000	1.8×10^{-1}	...	3.0×10^3
Stanford (SCA recirculator)	20–200	5 (25)[d]	8.0×10^{-4}	0.02	1.6×10^6
NIST (race-track microtron)	17–185	(2 – 4)[d]	$(1.0 \times 10^{-3})^d$	40 keV[i]	8×10^5
LANL (rf linac/HIBAF)	17	280	3.5×10^{-3}	0.5	4.6×10^6

[a] Peak current.

[b] $\epsilon_n = 4\epsilon_{n,rms} = 4\left[\langle x^2\rangle\langle(p_x/m_0c)^2\rangle - \langle xp_x/m_0c)^2\rangle\right]^{1/2}$.

[c] $B_n = 2I_b/\pi^2\epsilon_{x,n}\epsilon_{y,n}$.

[d] Designed upgrade value.

[e] The FWHM normalized emittances in the horizontal and vertical directions are 8×10^{-4} cm rad and 4×10^{-4} cm rad, respectively.

[f] The longitudinal emittance is 30 keV ps. The electron pulse length can be 1–6 ps.

[g] This is the core brightness. The edge brightness would be approximately a factor of 2 lower.

[h] Measured normalized rms emittance is $\pi\epsilon_{n,rms} = 6 \times 10^{-2}$ cm rad. Used $\epsilon_n = 3\epsilon_{n,rms}$ and $B_n = 2I_b/9\pi^2\epsilon_{n,rms}^2$.

[i] Same for all energies.

[j] Design parameters.

Table III: Explicit Conditions for Guided Radiation Beam in the Compton Exponential Gain Regime

	Gaussian Electron Beam	Parabolic Electron Beam
Filling factor, $f = \frac{\sigma_b}{\sigma_r}$	$\frac{\sqrt{3}}{2}\left(\frac{3\sqrt{2}k\Gamma_0\sigma_b}{5\pi}\right)^{1/3} - \frac{1}{6}$	$\frac{3}{4}\left(\frac{3\sqrt{2}k\Gamma_0\sigma_b}{5\pi}\right)^{1/3}$
Radius of Curvature, R	$-\frac{k\sigma_b}{2\pi}\frac{(3f+2)^{1/2}}{f^{3/2}}$	$-\frac{k\sigma_b}{\pi}\frac{(6f-1)^{1/2}}{f(2f-1)^{1/2}}$
Growth rate, Γ	$\frac{6\sqrt{2}}{5}\Gamma_0\frac{3f+2}{(2f+1)^2}$	$\frac{3}{5}\Gamma_0\frac{(6f-1)}{f(4f-1)}$
Phase shift, Δ	$\frac{6\sqrt{2}}{5}\Gamma_0\frac{f^{1/2}(3f+2)^{1/2}}{(2f+1)^2}$	$\frac{3}{5}\Gamma_0\frac{(2f-1)}{f(4f-1)}$
Intrinsic efficiency, η	$\Delta k/k_u$	$\Delta k/k_u$
Area of e-beam, σ_b	πr_b^2	$\pi r_b^2/2$

$$\Gamma_0 = \frac{5}{6}\frac{f_B K k_u}{(1+K^2)^{1/2}}\left(\frac{\nu}{\gamma_0}\right)^{1/2}$$

$\nu = I_b/17\beta_0$ Budker's parameter
I_b peak current in kA
$k = 2\gamma_0^2 k_u/(1+K^2)$ radiation wave number
r_b electron beam radius
$f_B = J_0(b) - J_1(b)$
$K = (|e|/m_0c^2)(A_u/\sqrt{2})$
$b = K^2/2(1+K^2)$
$\beta_0 = (1-\gamma_0^{-2})^{1/2}$

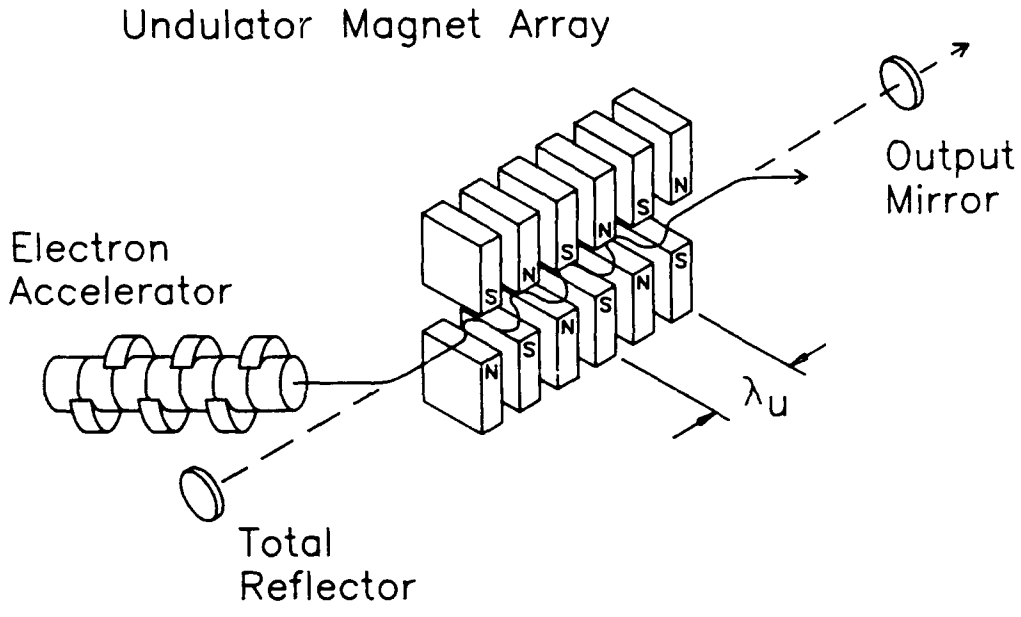

Fig. 1 — Schematic of an FEL consisting of an electron beam, an undulator and the radiation, in an oscillator configuration

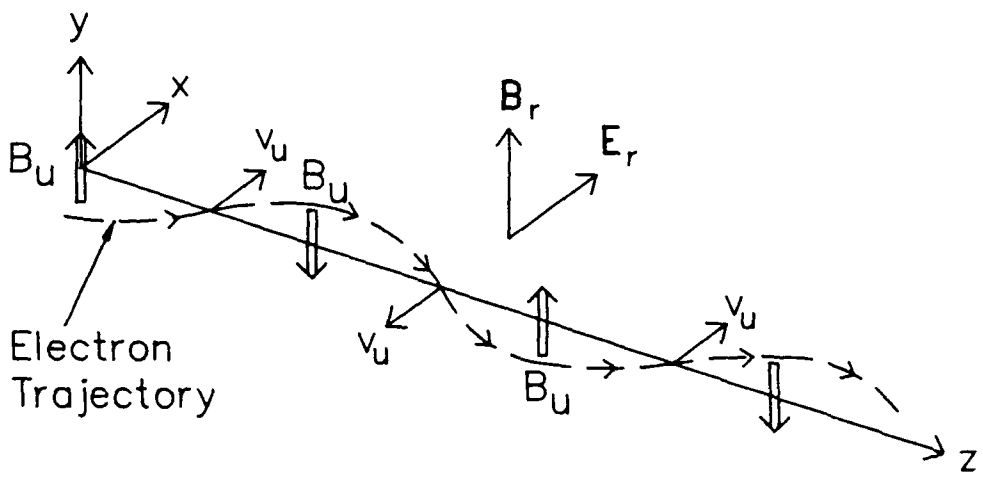

Fig. 2 — Configuration of large amplitude electron motion in the fields of the undulator

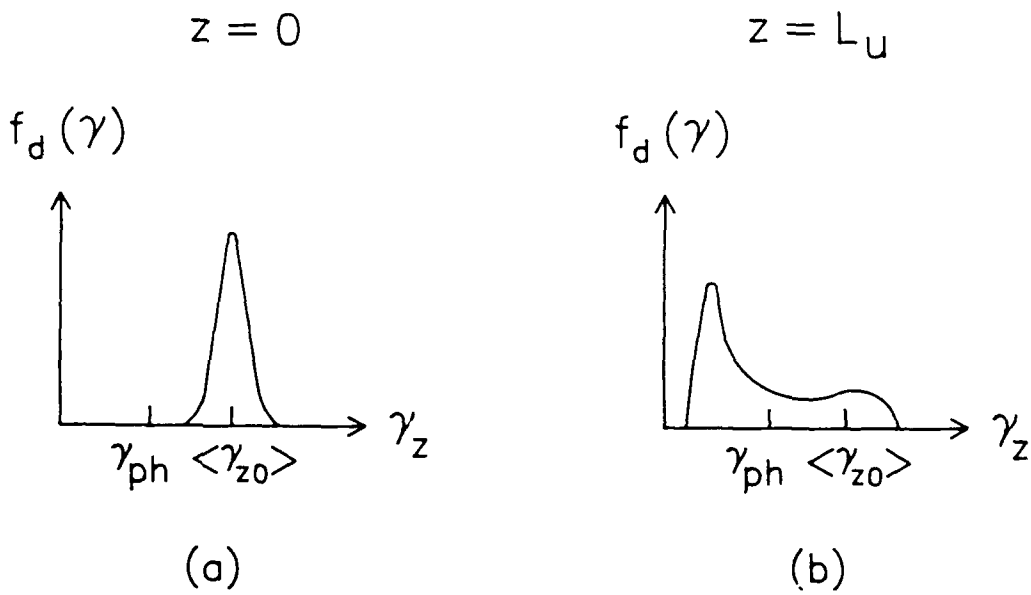

Fig. 3 — Distribution function of electrons at the entrance and exit of a uniform undulator for an FEL with high gain

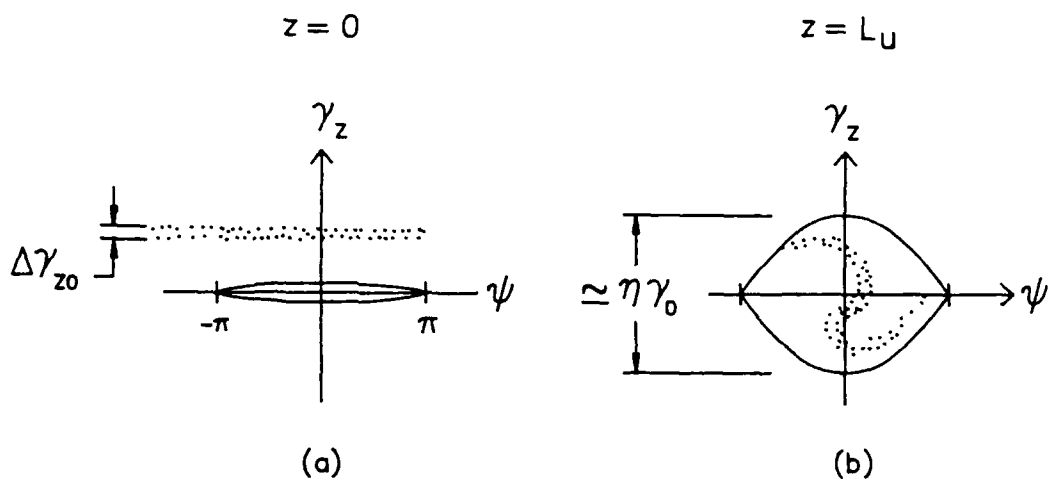

Fig. 4 — Phase space diagram of electrons at the entrance and exit of a uniform undulator for an FEL with high gain

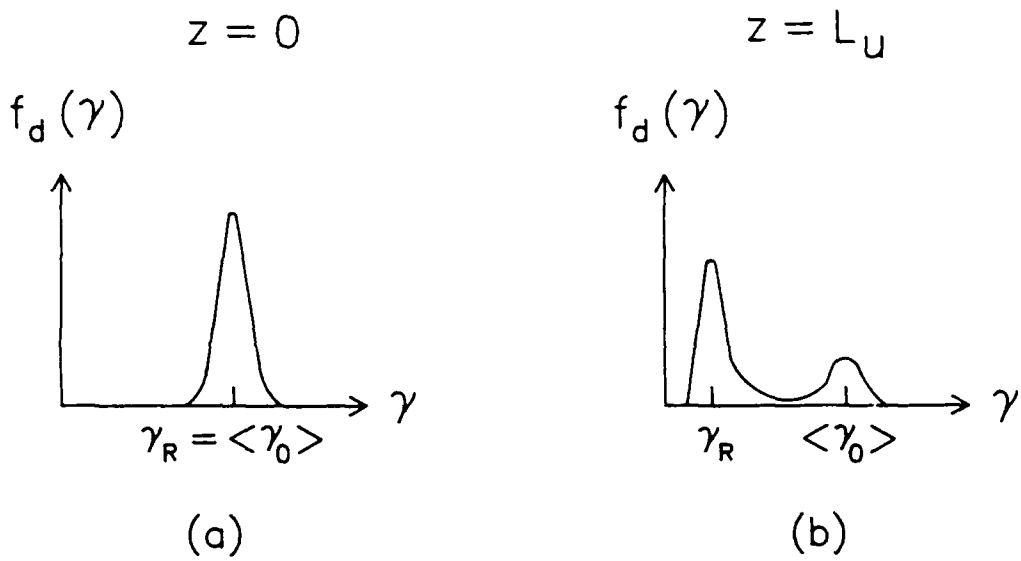

Fig. 5 — Distribution function of electrons at the entrance and exit of a tapered undulator

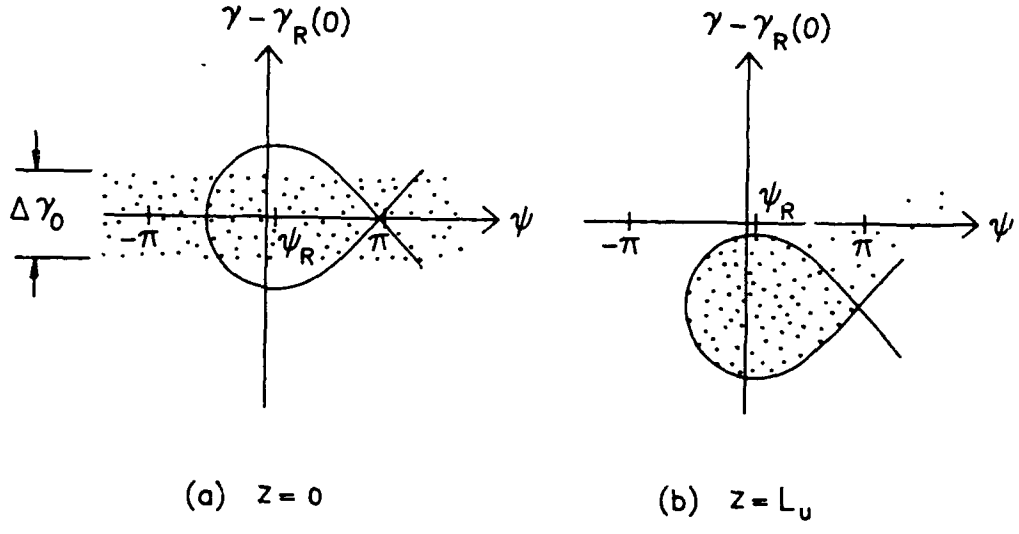

Fig. 6 — Phase-space diagram of electrons at the entrance and exit of a tapered undulator

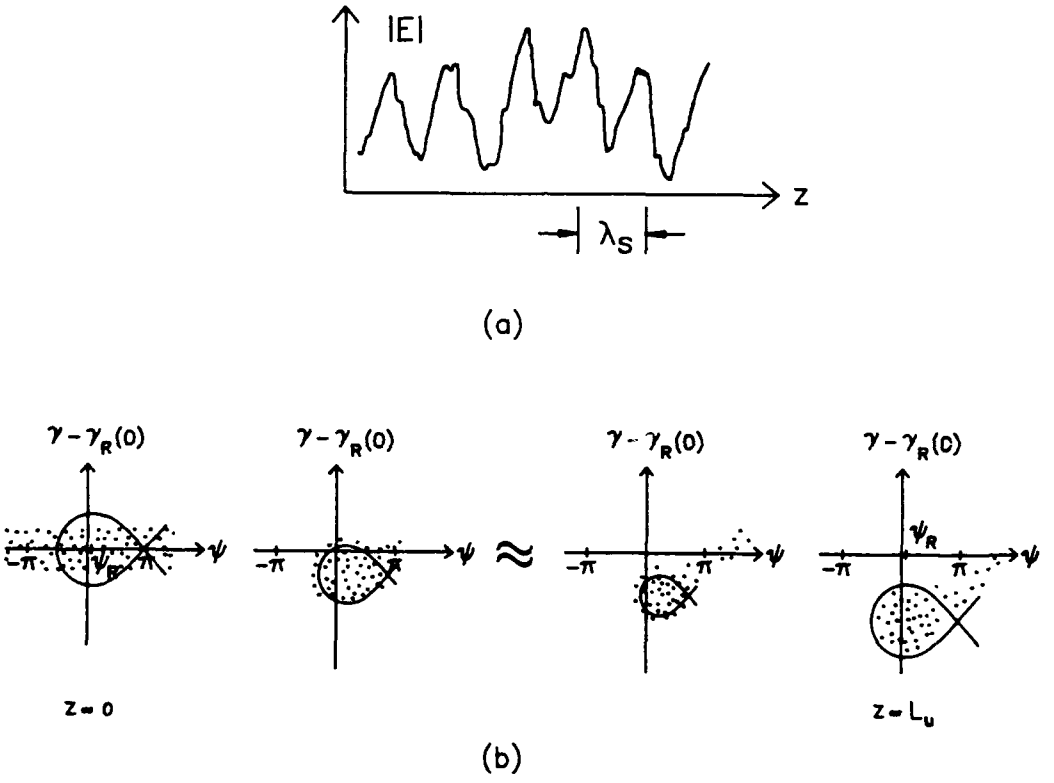

Fig. 7 — (a) Radiation amplitude modulated by sidebands, and (b) oscillation of the separatrix as a result of the modulated radiation amplitude

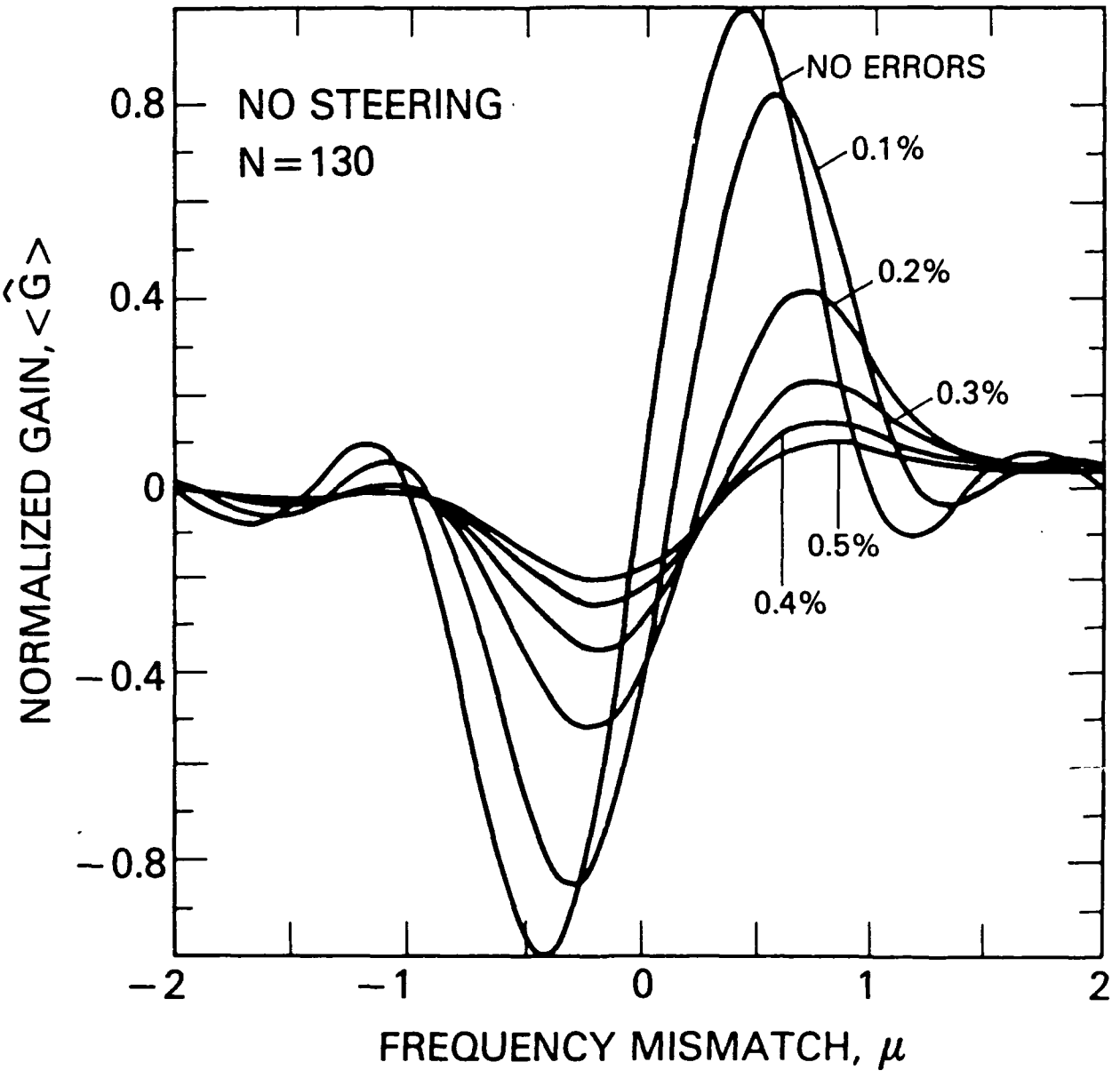

Fig. 8 — Mean normalized gain, $\langle \hat{G} \rangle$, versus frequency mismatch, μ, for several values of rms field error, $\delta \hat{B}_{rms}$, for a linearly polarized undulator with B_u = 5.4 kG, λ_u = 2.8 cm, L_u = 3.6 m, and γ = 350 in the limit $k_\beta = 0$

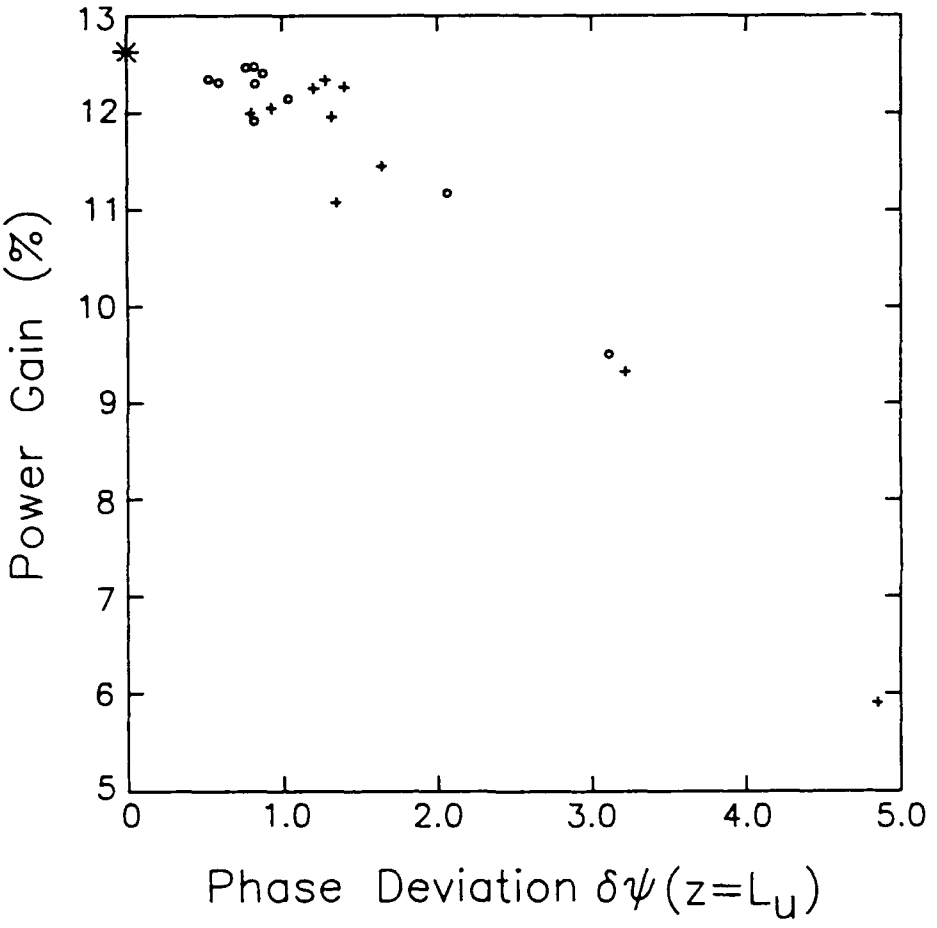

Fig. 9 — Plot of gain versus phase deviation for different field errors: (*) no magnetic field errors, (○) $(\Delta B/B)_{rms} = 0.4\%$, and (+) $(\Delta B/B)_{rms} = 0.5\%$. The same random number seeds are used for (○) and (+)

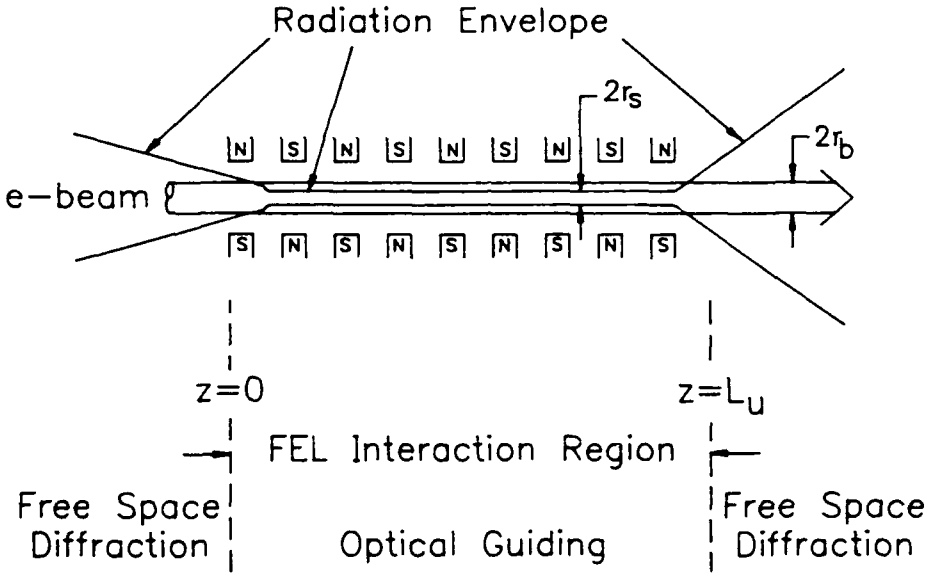

Fig. 10 — Schematic of an FEL where the radiation is "perfectly" guided in the interaction region

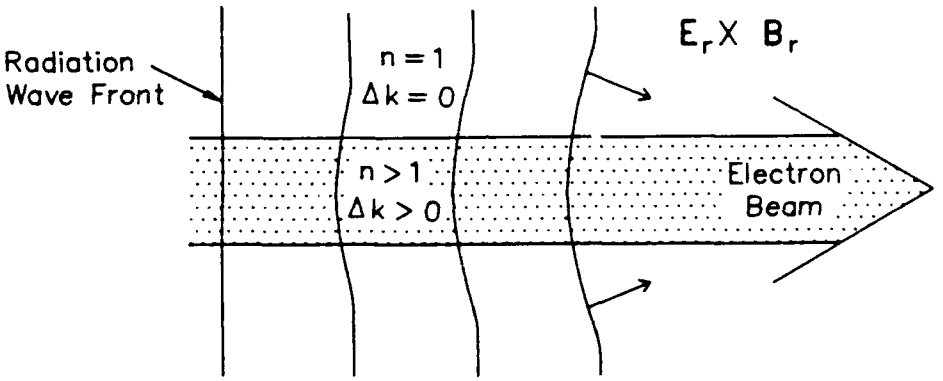

Fig. 11 — Schematic illustrating the refractive property of the FEL in the low gain regime